Master's Degree in Chemical Engineering

Hydrodynamic modelling of valve trays

Master Thesis

From

Joana Cristina de Almeida Ferreira

Development within the course of Dissertation

Held in

IFP-Energie Nouvelles

Supervisor of FEUP: **Prof.Jose Carlos Lopes**

Supervisor: **Dra.Aude Royon-Lebeaud**

Department of Chemical Engineering

July of 2014

"Persistence is the road to accomplishment."

(Charles Chaplin)

Acknowledgements

I would like to thank to IFP Energie nouvelles for the opportunity to make the dissertation in a business environment, on an internship program. To Prof. Miguel Madeira I would like to acknowledge for helping and encouraging for the entrepreneurship.

I am thankful to Drª. Aude Royon-Lebeaude, my supervisor at the company, for her support and orientation. For believing in me and for all the times she showed that everything is possible with work and dedication.

To my supervisor at FEUP, Prof. José Carlos Lopes, I would like to thank for providing his support for what was needed and availability

Huge thanks to Rim Brahem, for her friendliness, for always helping me when I needed. To her, my sincere thanks. To my colleagues from IFPen, who helped me and supported me during the past five months.

To my colleagues from the university a huge thanks you for their friendship, companionship and help during these five years. Thank you for all the times we spent together, for your support and encouraged me when needed.

I am especially grateful to my boyfriend for the daily support, in good and bad moments and for encouraging me when needed. For the comprehension and strength demonstrated at all times.

Last but not least, to my family, especially my parents, a huge thank you for all the love, support and dedication they constantly offered me. For all the opportunities they have given me, for helping me all the times and encouraging me.

Abstract

Natural gas demand continues to increase. However around 40 % of the world's natural gas resources are raw natural gas with high concentrations of hydrogen sulphide (H_2S) and/or carbon dioxide (CO_2) (above 20% by volume). The most used gas sweetening process is absorption with amine solutions. This process consists of two main units: a counter current gas-liquid absorption column in which acid compounds are removed from the gas and a stripper column for loaded solvent regeneration.

An optimisation is needed to reduce the over-sizing costs and enhance efficiency especially for the absorber column. The column optimization passes through the optimization of gas-liquid contractors liquid contactors used in gas absorption column. For this a study of hydrodynamics and mass transfer parameters is important.

The flow over these contractors, and in particular over a tray, is very complex. An approach based on complementarity between experimental tools and CFD simulations gived access to a more detailed description and a deeper understanding of the hydrodynamic and mass transfer.

The use of CFD present various advantages such as: less dependence of pilot installations, the independent study of the influence of several parameters including geometric and physic-chemical parameters. These advantages promote the interest for extrapolation to industrial scale.

In this work comparison between the experimental, theoretical and simulations are first made for a simulation with gas only. The simulations results for the pressure drop showed a good approximation to experimental and theoretical values. The simulations provide clear knowledge of gas flow, which is helpful for the two phase's simulations.

Secondly the gas/liquid flow is simulated with a two phase eulerian model. The interection between gas and liquid was modelled as a drag force. Different geometries, boundary conditions and drag force coefficient were tested. The best approach is the geometry where the exit of gas is the holes of the valves for the "tray above". The boundary conditions are pressure outlet for gas and liquid and velocity inlet for gas and liquid. The schiller-naumann interaction was used. The VOF simulation was done to tracks the interphase between the two phases. Both proved the possibility to understanding the two phase flow behaviour.

Keywords: Hydrodynamic, Absorption, Tray column, CFD, Euler-Euler

Resumo

A procura de gás natural como energia continua a aumentar. No entanto cerca de 40% dos recursos de gás natural do mundo são compostos com altas concentrações de ácido sulfúrico (H_2S) e /ou dióxido de carbono (CO_2) (acima de 20% em volume). A absorção com aminas é o processo mais utilizado para remover os ácidos contidos no gás. Este processo consiste em duas unidades principais: uma coluna de absorção em contracorrente de gás-líquido, em que os compostos ácidos são removidos do gás e uma coluna de remoção (stripping) para a regeneração do solvente.

A otimização de coluna de absorção é necessária para reduzir os custos relacionados com o dimensionamento e a eficiência da mesma. A otimização da coluna passa pela otimização das válvulas utilizadas na coluna de absorção de gás. Para tal um estudo dos parâmetros hidrodinâmicos e de transferência de massa é necessário.

O estudo do escoamento em válvulas é extremamente complexo. Como tal o uso da modelização em CFD associado aos dados experimentais torna-se uma ferramenta essencial para a aproximação dos parâmetros hidrodinâmicos e para a compreensão do escoamento.

O uso de CFD apresenta várias vantagens, tais como: menor dependência de instalações piloto, o estudo independente da influência de diversos parâmetros, incluindo parâmetros geométricos e físico-químicos. Essas vantagens promovem o interesse para a extrapolação à escala industrial.

Neste trabalho foram realizadas comparações entre os resultados experimentais, teóricos e simulações unicamente com gás. Os resultados das mesmas relativamente à queda de pressão mostraram uma boa aproximação aos valores experimentais e teóricos. As simulações fornecem um conhecimento sobre o escoamento gasoso útil para futuras simulações entre duas fases.

Foram realizadas simulações gás/liquido com o modelo eulerian. A interação entre o gás e o líquido é modelizada através de um coeficiente de arrasto. Foram testadas diferentes geometrias, condições de fronteira e coeficientes de interação gás-liquido. A melhor abordagem é com a geometria, onde a saída de gás é através das válvulas do "prato superior". Foram tidas em consideração pressões á saída do gás e do líquido e imposta uma velocidade de entrada para os mesmos, assim como a interação Schiller-Naumann. A simulação com o método VOF é utilizada para observar a interface entre o gás e o líquido. Ambos provaram a possibilidade de compreender o comportamento do fluxo de duas fases.

Palavras-chave: Hidrodinâmica, Absorção, Coluna de pratos, CFD, Euler-Euler

Declaration of Honour

Declare, on oath, that this work is original and that all non-original contributions were properly referenced with identifying the source.

Joana Cristina Almeida Ferreira

4th July 2014

Index

List of Figures

List of Tables

Notation and Acronyms

A_a	Active area	m^2
A_h	Perforate area	m^2
a_e	Exchange area	m^2
A_t	Total area	m^2
C_D	Drag Coefficient	--
F_a	Kinetic factor of gas for the active area	$Pa^{0.5}$
F_s	Kinetic factor of gas for the section of column	$Pa^{0.5}$
g	Gravity acceleration	ms^{-2}
h_{cl}	Clear liquid height	m
h_{Fe}	Emulsion height	m
h_w	Weir height	m
L_p	Lager of tray	m
L_w	Lager of weir	m
Q_L	Liquid flowrate	m^3s^{-1}
Q_G	Gas flowrate	m^3s^{-1}
U_G	Gas velocity	ms^{-1}
U_{Ga}	Gas velocity in the active area	ms^{-1}
U_{Gh}	Gas velocity in the perforate area	ms^{-1}
α_G	Gas retention	--
α_L	Liquid retention	--
Δp	Pressure drop	Pa

Greek Letters

ρG	Density of gas	Kgm^{-3}
ρL	Density of liquid	Kgm^{-3}
μ	Viscosity	Pa.s

Acronyms List

IFPEN	IFP Énergies Nouvelles
CFD	Computational Fluid Dynamics
VOF	Volume of Fluid
Co_2	Carbone dioxide
H_2S	hydrogen sulphide

1 Introduction

In this chapter, is presented some data about the evolution of mix energy in the word, with more interest in the natural gas. Second point is the presentation and aim of the project. The last point is a company description.

1.1 Project Presentation and aim

Natural gas will continue to increase its share of the global energy mix, growing at 2.4% per year until 2018 (iea, 2014). Figure 1 represents the consumption of natural gas in the next years (Brahem, 2013).

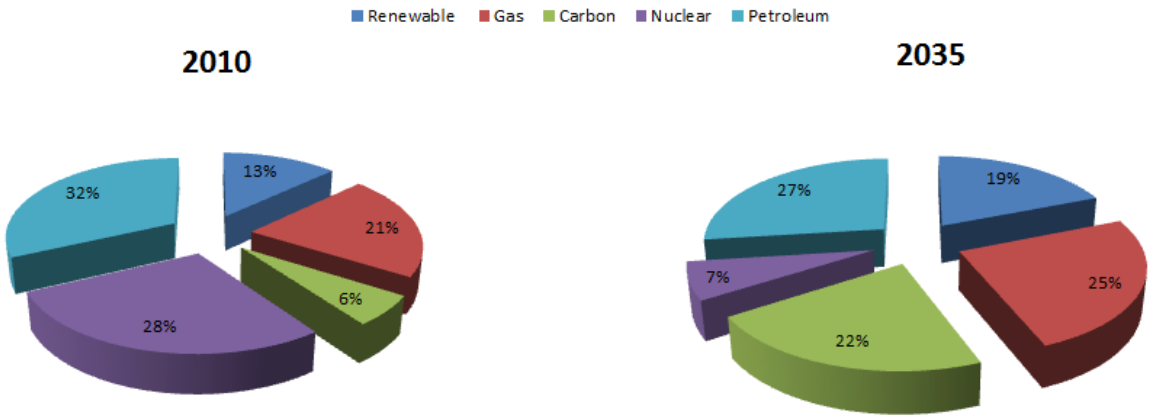

Figure 1- Global energy mix evolution (Brahem, 2013)

The natural gas used by consumers is significantly different from the natural gas that is brought up from the gas well. Natural gas processing consists of separating all of the various hydrocarbons and impurities from the raw natural gas to produce a natural gas almost composed by methane.

Around 40 % of the world's natural gas resources are raw natural gas with high concentrations of hydrogen sulphide (H_2S) and/or carbon dioxide (CO_2) (above 20% by volume). The presence of theses acid compounds causes environmental and operational problems.

For the commercialization of this gas the requirements on the product compositions must be satisfied.

A techno-economic study by IFPEN (Ludovic Raynal et al., 2012) shows a flowchart of process for CO_2 capture, similar to the process equipment in gas processing. The investment cost of the column absorption is about 40% of the process. For a treatment of acid gas the investment cost share up to 50%.

The process is largely limited by the phenomenon of mass transfer. An optimization of the absorbers design could significantly decreases the cost of the process.

The column optimization passes through the optimization of liquid contractors used in gas absorption column.

Under this context the project passes through the study in a counter current gas-liquid absorption column in which acid compounds are removed from the gas.

Particularly understand the scale effect of the hydrodynamics on valve trays contractors used in the absorption column. The principal large objectives are:

- Fit the closure law for the drag force to be available experimental data and understand the evolution of the C_D (drag force coefficient) with the hydrodynamics parameter.
- Realize CFD (Computational Fluid Dynamic) simulations for different lengths to ensure extrapolation to industrial scale.

1.2 Company description

IFP Energies nouvelles (IFPEN) is a public research and training player. It has an international scope, covering the fields of energy, transport and the environment. From research to industry, technological innovation is central to all its activities.

As part of the public-interest mission with which it has been tasked by the public authorities, IFPEN focuses on:

- Providing solutions to take up the challenges facing society in terms of energy and the climate, promoting the emergence of a sustainable energy mix;
- Creating wealth and jobs by supporting French and European economic activity, and the competitiveness of related industrial sectors.

Its programs are hinged around 5 complementary, inextricably-linked strategic priorities:

- **renewable energies**: producing fuels, chemical intermediates and energy from renewable sources;
- **eco-friendly production**: producing energy while mitigating the environmental footprint;
- **innovative transport**: developing fuel-efficient, environmentally-friendly transport,
- **eco-efficient processes**: producing environmentally-friendly fuels and chemical intermediates from fossil resources;

- **Sustainable resources**: providing environmentally-friendly technologies and pushing back the current boundaries of oil and gas reserves;

An integral part of IFPEN, its graduate engineering school prepares future generations to take up these challenges.

1.3 These Organization

The work is composed by 7 chapters. The first chapter is an introduction to the project, where the aim and the main goals are presented and the description of the company.

The second chapter expose the context of the project, in which is explained the fundamental concepts of absorption columns, particularly the concepts related with valve trays. Also a description of the existing pilot unites in the laboratory (Experimental Set-up) is included.

The third chapter is related with simulation modelling/State of art. In this chapter is present the concepts about multiphase flows, the Euler-Euler approached and interaction gas-liquid. Some important works done in the last years are referenced.

In the fourth chapter is made a description of the geometry with all details, used for the project. Fifth (Hydrodynamic modelling: Gas) and sixth (Hydrodynamic modelling: Gas-Liquid) chapters are the most important, in these chapters some concepts related with the hydrodynamics variables are presented, the results of simulations are compared with experimental and theoretical values and the discussion of these results is exposed.

The seventh chapter is a final conclusion of all the work, with some future perspectives. The last is the bibliography.

2 Context

2.1 Gas treatment

Actually there are several technologies commercially available to treat acid gases. The classification of these technologies depends on the removal mechanism .They are typically based upon the absorption of CO_2 by means of a chemical or physical solvent.

The major differences of these technologies are:

- Absorption: Chemical or physical, with/without desorption
- Adsorption: Chemical or physical, with/without desorption
- Permeability

These differences determine the main advantages and disadvantages of each technology. The sweetening technologies can be briefly classified according to the following Table 1:

Table 1- Classification of sweetening technologies (M. & I., 2009)

Removal Mechanism	Process Type	Technology	Commercial name
Chemical Absorption	Regenerative, continuous	Amines	Monoethanolamine and other formulated solvents
		Potassium carbonate	Benfield,Catacarb,Giammarco-Vetrocoke,etc.
	Nom regenerative, continuous (usual arrangement: lead/lag)	Sodium hydroxide	-
Physical Absorption	Regenerative, continuous	Physical solvents	Selexol, Rectisol, Purisol, Fluor Solvent, IFPexol, etc.
Physical-chemical absorption	Regenerative, continuous	Physical-chemical solvents	Sulfinol, Ucarsol LE 701, 702 e 703, FlexSorb PS,etc
Physical adsorption	Regenerative, continuous (adsorption/desorption sequence)	Molecular sieves	Z5A (Zeochem), (UOP), etc.
Permeation	Continuous	Membranes	Separex, Cynara, Z-top, Medal,etc.

The first approach to select a technology available to treat the gases depends on the quantity of gaseous acid in the gas to treat. The most comprehensive process, covering a large range of concentrations is absorption with amines (M. & I., 2009).

Absorption is one of the oldest unit operations used in the gas processing industry. Acid gas enters the bottom of the absorber and flows upward contacting the countercurrent liquid

stream. The liquid preferably absorbs the heavier components from the gas, which are mainly acid compounds. Next, the liquid with acid compounds is sent to a stripper where the absorbed components are removed by heating and/or stripping with steam. The liquid, now clean is recycled to the absorber to complete the process loop.

For a given gas, the fraction of each component in the gas that is absorbed by the liquid is a function of the equilibrium phase relationship of the components and liquid, the flow rates, and the contact stages. The phase relationship is a function of pressure, temperature, and the composition of the clean liquid. The stripping column is operated at low pressure and high temperatures.

A typical amine system is show in Figure 2 (Stewart & Arnold, Gas Sweetening and Processing Field Manual , 2011). This process consists of two main units: a countercurrent gas-liquid absorption column in which acid compounds are removed from the gas and a stripper for loaded solvent regeneration.

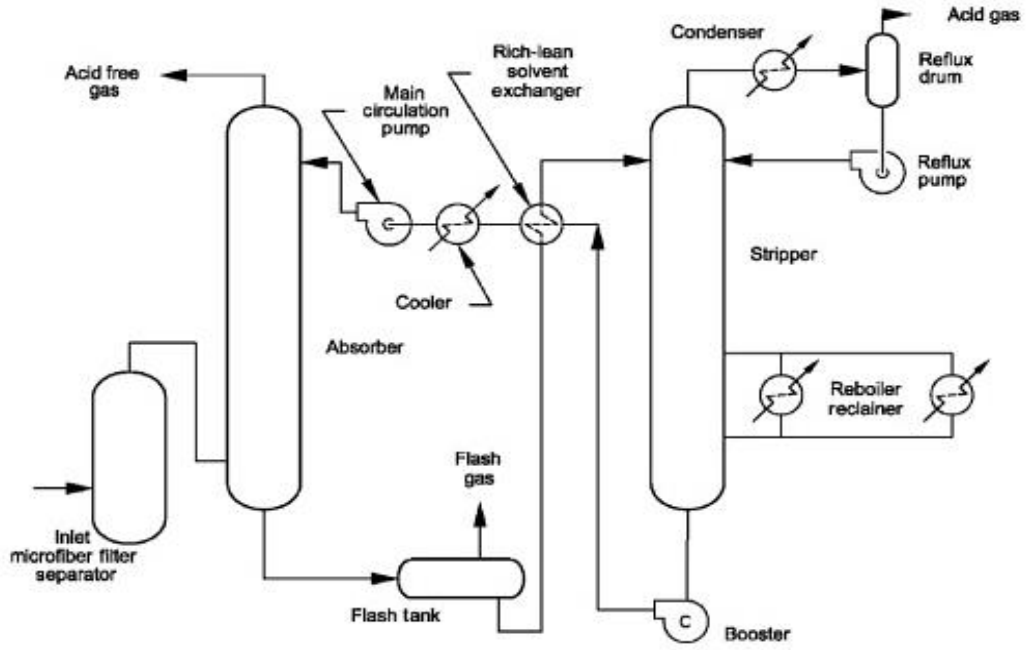

Figure 2- Example of a Column Absorption and Stripper (Stewart & Arnold, Gas Sweetening and Processing Field Manual , 2011)

2.2 Technology tray

The dimensioning of a tray column essentially requires the determination of the total height and the column diameter. These two parameters have direct impact in the cost of the column and thus the cost of the process.

The total height is based on the number of trays required to achieve the product specifications imposed. This number depends on the number of theoretical stages required by thermodynamics and transfer efficiency on the tray. The efficiency is a function of interfacial area exchange (a_e) and the mass transfer coefficients in the liquid and gas side. A good prediction of these parameters is essential for optimal sizing of the column height.

Some hydrodynamic operating conditions decrease the efficiency of the column and make the column inoperable.

For a lower velocity of the gas, the liquid passes through the holes tray (weeping). Such operation degrades efficiency of the column. For a higher velocity the liquid droplets are entrained with the gas to the tray. The liquid is accumulated in the column and it becomes inoperable and the performance decrease.

A tray column consists of single trays adjusted one over the other. An appropriate tray intensifies the phases contact and increase the mass transfer between the two phases. A scheme of the geometry is illustrated in Figure 3.

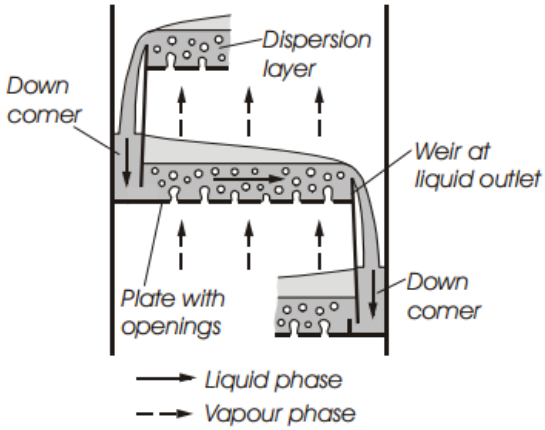

Figure 3- Scheme of geometry for the trays absorption (Gamse, 2010)

The principal elements of a tray column are:

- **Trays:** area of contact between the two phases, where the transference occurs, and different sections can be identified:
    - Active area (Aa): Correspond to the section where the gas and liquid are in contact.
    - Perforated area (A_h): Is the area of where the tray is open.
    - Dead area: Is the area where the tray doesn't have perforations, generally near the walls.

- **Donwcomers:** Compile different functions. First is liquid flow, second the separations of the two phases
- **Weir:** secures the height of liquid above the tray.

Figure 3 above presents a column in countercurrent flow, where the liquid direction is defined as a single pass cross flow; the liquid flow across the tray from the inlet to the outlet and from the top to the bottom of the column. The liquid enriches with acids compounds and flowing over each single tray. The gaseous phase passes in the open areas of the tray, enters the liquid phase and disperses into the liquid.

Other important characteristic of these columns is the type of gas phase inlet. According to the liquid direction, different possibilities for the gas phase inlet can be applied such as: Tunnel tray, Bubble cap tray, Sieve tray, Valve tray, etc.

The valve tray was the type used for this work (see Figure 4). This type of valve presents different advantages such as:

- High velocity of the gas phase, and contact with the liquid phase;
- Possible lower pressure drop;
- Variability of the outlet opening area for different gas loadings;
- High efficiency and flexibility

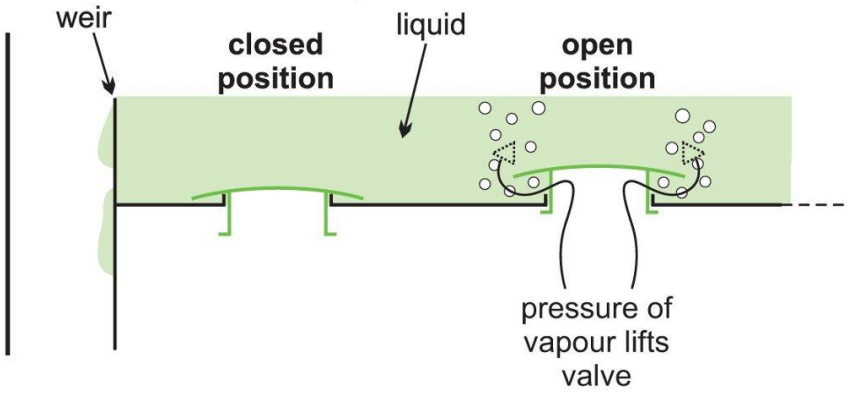

Figure 4-Different positions of the valves.

An excellent design of the column requires control of the hydrodynamics and transfer parameters. The usual approach of process engineering is to study at laboratory scale and after compare the results with computational simulations. Extrapolation of the results on an industrial scale is the last step.

2.3 Experimental Set-Up

Two rectangular columns 2 meters of height and equipped with 4 valve trays each were made available to carry out all the hydrodynamic and interfacial area tests (see Figure 5). The columns are made of Plexiglas and are completely transparent to enable the visualization of flow. Each column has four trays equipped with V4R Glitsch valves.

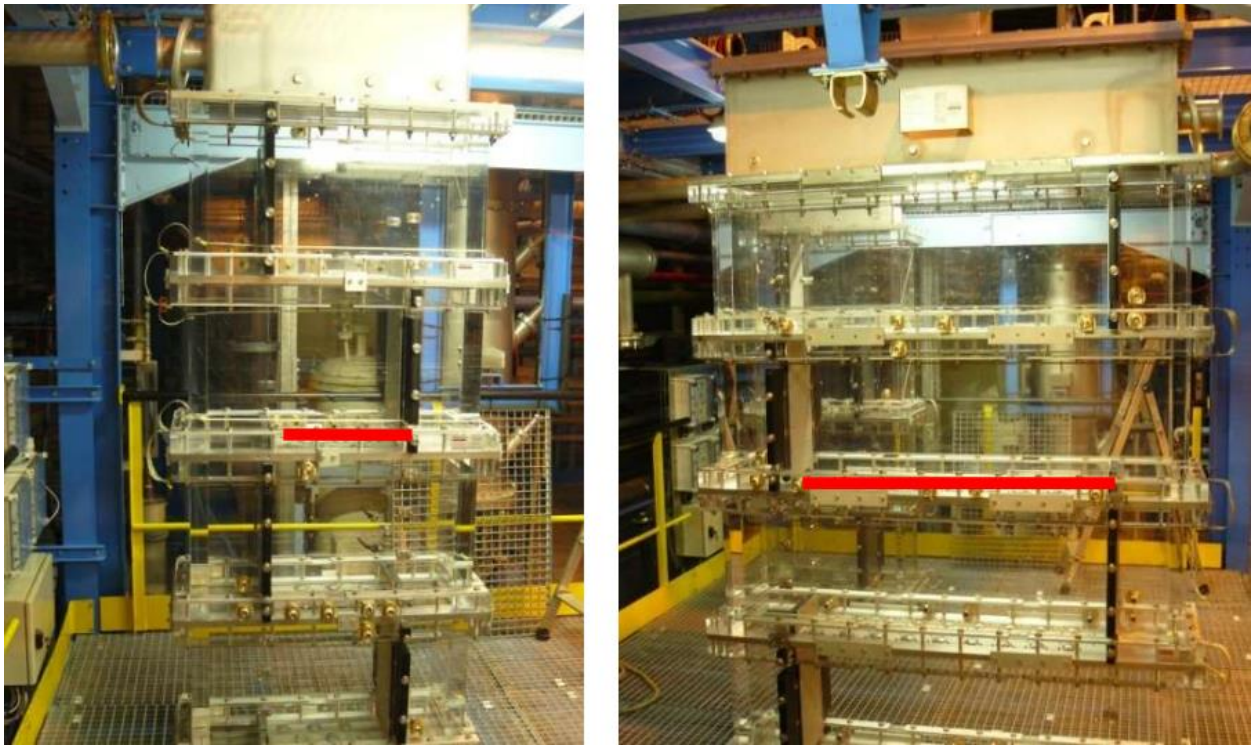

Figure 5- Pictures of the two columns of unit U717B (IFPen department Lapis-Lazuli)

The geometrical characteristics of the two columns are identical except for the length of pass L_P (see the geometrical characteristics of the two columns in Table 2).

The rectangular columns are assumed to be equivalent to a 2D cross section of a circular column with a diameter equal to the total length D.

The two columns operate with the same utilities. Both columns operate with a gas / liquid flow in counter-current. The liquid is used in a closed loop on the unit and it is stored in two tanks with a total capacity of 1100 L.

The unit is equipped with:

- Mass flowrate liquid and gas.
- Nanometers for measuring pressure drop.
- Infrared sensors for measuring concentrations of carbon dioxide CO_2 in air.

Both columns operate at atmospheric pressure and room temperature in a water / air system.

Table 2-Geometric characteristics of the two columns (Brahem, 2013)

Tray characteristics		
	Column 1	Column 2
Total larger (m)	0,66	1,26
Lager of tray Lp (m)	0,36	0,96
Total section AT (m^2)	0,13	0,24
Active Area A_a (m^2)	0,07	0,18
Hole area A_h (m^2)	0,011	0,032
Height of weir h_w (m)	0,065	
Large of weir L_w (m)	0,1905	
Number of trays	4	
Valves characteristics		
Type	V4R GLITSCH	
Number of valves/ tray	9	27
Minimum height (m)	0,001	
Maximum height (m)	0,009	
Diameter of valve (m)	0,0475	
Diameter of hole (m)	0,039	
Valves / air active	122	

3 Model Simulation: State of Art

Several works about CFD simulations have been done along the past years. Some of them are described in this chapter. This chapter contains a revision of the principal concepts; the most important works are discussed, as same important results. Different characteristics between the presented important works are described.

3.1 Computational Fluid Dynamic (CFD)

The study of the hydrodynamic flows is difficult. So the use of CFD for modelling the hydrodynamics flow in partnership with experimental results give us good approximations for hydrodynamic parameters.

The uses of CFD present various advantages such as: less dependence of pilot installations, the independent study of the influence of several parameters including geometric and physic-chemical and a better description of the hydrodynamics parameters (Zarei A. R., 2012). These advantages promote the interest for extrapolation to industrial scale.

3.1.1 Multiphase Flow

The materials presented in multiphase flow are often identified as belonging to the primary or secondary phases. The primary phase is characterized as a continuous phase. The secondary phase is thought to be the material that is distributed throughout the primary phase.

Multiphase flow modelling with CFD poses a combination of challenges that are unique to this type of problem. The first important issue is how to choose a multiphase model that will be used to compute solutions.

An appropriate selection must be made for the multiphase model to ensure that the program is able to use the correct continuity equations and also apply them to the fluids in a way that most accurately mimics real-life fluid flow.

3.1.2 The Euler-Euler Approach

The Euler-Euler approach introduces the concept of phasic volume fraction. Volume fractions are assumed to be continuous functions of space and time and their sum is equal to one. Notice that the volume of one phase cannot be occupied by other phases. Conservation equations for each phase are derived.

Two different multiphase models are available and of interest: Eulerian-Eulerian model and Volume of Fluid (VOF) model.

- Eulerian-Eulerian Model: Primary and secondary phases are treated individually as being continuous and separate momentum equations are solved for each phase. Coupling is achieved through the pressure and interphase exchange coefficients.

- Volume of Fluid (VOF) Model: An Eulerian-Eulerian variation in which the secondary phase is not dispersed within the primary phase but rather there is an interface between the phases and so the interface must be tracked while also solving a conservation and momentum equation.

The VOF model is not able to represent a large interaction surface, and generally VOF models does not provide good results for a large geometry. More details about these models are present below.

3.1.2.1 Eulerian-Eulerian model

For Eulerian-Eulerian simulations the dispersive gas and continuous liquid phase were modelled as two interpenetrating phases having separate transport equations. The continuity (equations 3-1 and 3-2), momentum (equations 3-3 and 3-4) and mass transfer equations were numerically solved for each phase.

Continuity equation for the gas phase:

$$\frac{\mathrm{d}(\alpha_{\mathrm{G}}\rho_{\mathrm{G}})}{\mathrm{dt}} + \nabla.(\alpha_{\mathrm{G}}\rho_{\mathrm{G}}\vec{u}_{\mathrm{G}}) = 0 \qquad \textit{3-1}$$

Continuity equation for the liquid phase:

$$\frac{\mathrm{d}(\alpha_{\mathrm{L}}\rho_{\mathrm{L}})}{\mathrm{dt}} + \nabla.(\alpha_{\mathrm{L}}\rho_{\mathrm{L}}\vec{u}_{\mathrm{L}}) = 0 \qquad \textit{3-2}$$

Where α_G or α_L are the volume fraction for gas and liquid and their sum is equal to 1.

Momentum equations for gas phase:

$$\frac{\mathrm{d}(\alpha_{\mathrm{G}}\rho_{\mathrm{G}}\vec{u}_{\mathrm{G}})}{\mathrm{dt}} + \nabla.(\alpha_{\mathrm{G}}(\rho_{\mathrm{G}}\vec{u}_{\mathrm{G}}\vec{u}_{\mathrm{G}})) = \nabla.(\alpha_{\mathrm{G}}\mu_{\mathrm{eff,G}}\left(\nabla\vec{u}_{\mathrm{G}} + (\nabla\vec{u}_{\mathrm{G}})^{\mathrm{T}}\right) - \alpha_{\mathrm{G}}\nabla p_{\mathrm{G}} - \mathrm{M}_{\mathrm{GL}} + \alpha_{\mathrm{G}}\rho_{\mathrm{G}}\vec{g} \qquad \textit{3-3}$$

Momentum equations for liquid phase:

$$\frac{\mathrm{d}(\alpha_{\mathrm{L}}\rho_{\mathrm{L}}\vec{u}_{\mathrm{L}})}{\mathrm{dt}} + \nabla.(\alpha_{\mathrm{L}}(\rho_{\mathrm{L}}\vec{u}_{\mathrm{L}}\vec{u}_{\mathrm{L}})) = \nabla.(\alpha_{\mathrm{L}}\mu_{\mathrm{eff,L}}\left(\nabla\vec{u}_{\mathrm{L}} + (\nabla\vec{u}_{\mathrm{L}})^{\mathrm{T}}\right) - \alpha_{\mathrm{L}}\nabla p_{\mathrm{L}} - \mathrm{M}_{\mathrm{GL}} + \alpha_{\mathrm{L}}\rho_{\mathrm{L}}\vec{g} \qquad \textit{3-4}$$

Where, u_L and u_G are, respectively the velocity vectors of liquid and gas phases, $\rho_G$and ρ_L are the gas and liquid densities, p is the pressure in the fluid phase, g the gravitational acceleration and M_{GL} the interfacial forces acting on each phase.

During the evolution and improvement of the CFD several significant studies were developed in the last years (Lianghua & Cui Juejian, 2008) (Zarei, Hossein, & Rahimi, 2012)

(Alizadehdakhel, Rahimi, & Alsairafi, 2010) (Rahimi, 2012).These studies try to understand the influence of certain parameters in the efficiency of the columns.

Generally the results of simulations are often compared to global variables, mainly with average value of the liquid retention (α_L) and clear liquid height (h_{cl}) on the tray. Variations in the flow rate of liquid or gas as well as the height of the weir are quite well described by the simulations.

For example the 3D two-phase approach predicts the occurrence of non-homogeneities on the tray. (Zarei, Hossein, & Rahimi, 2012) predicted the weeping for a perforated rectangular tray. Non-uniform height of clear liquid and retention profiles were observed for the lower limits of tray operation.

Simulations also provide a great way for a better understanding and better control of the extrapolation of pilot scale to industrial scale. Krishna et al (2003) perform simulations for two columns with different diameters (0.3 to 0.9 m). The results show that the height of clear liquid between the two columns is comparable. The simulations shows liquid recirculation loops increases with a bigger tray diameter. These results with an integrated model of mass transfer or heat result to better predict of the actual performance of industrial columns.

Two more recent works are described (Zarei, Hossein, & Rahimi, 2012) (Rahimi, 2012). The first work is the study of weeping rate in the rectangular sieve trays. An Eulerian simulation was adopted with a three dimensional steady state model; this work was developed to describe the two phase flow and mass transfer on the tray. The hydraulic parameters such as clear liquid height and froth height have an effect on the gas liquid phase and mass transfer rates between the two phases.

Figure 6 represents a profile of volume fraction of liquid for a front view.

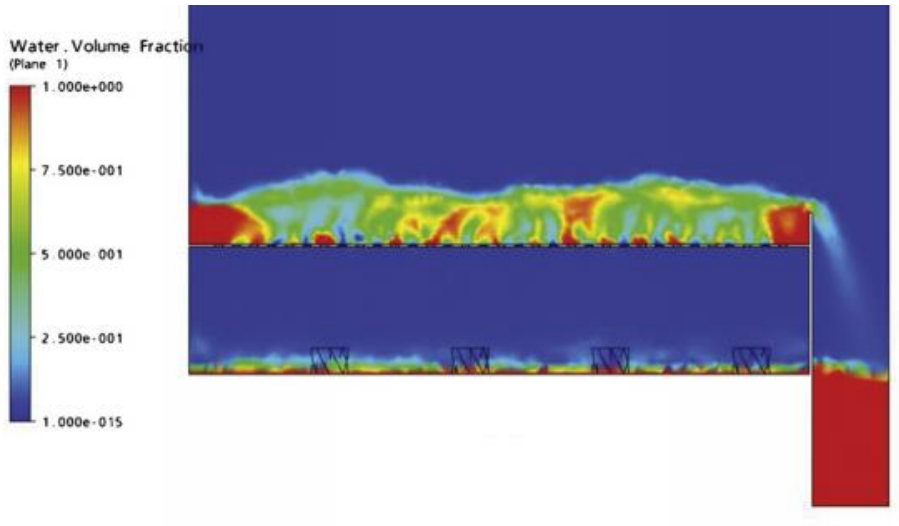

Figure 6- Profile of liquid volume fraction in a rectangular column (Zarei, Hossein, & Rahimi, 2012)

The clear liquid height is studied on the sieve tray at the weeping condition. Figure 7 shows a comparison between CFD and experimental results data from (Banik, 1986) in terms of clear liquid height against distance from the inlet downcomer. With a velocity (*Fs)* = 0.38 ms^{-1} and liquid flowrate (Q_l)= 0.000525m^3s^{-1}. The clear liquid height of rectangular sieve tray is non-uniform for both. So the CFD results are in agreement with experimental values. A model predicts an average error of 6.73 %.

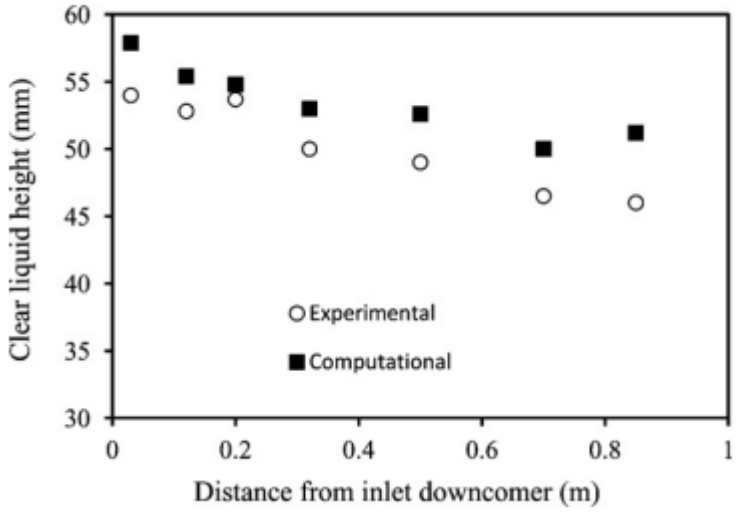

Figure 7-Comparison between the CFD results and experimental data of clear liquid height as a function of the distance from the inlet downcomer at Fs=0.38 ms^{-1} (Zarei, Hossein, & Rahimi, 2012)

The other work is related with the effect of the tray geometry on sieve tray efficiency the same concepts of Eulerian-Eulerian are used. They used two different geometries with different holes diameters. Figure 8 represent the froth height at *Fa* factor equal 0.4 $Pa^{0.5}$ and

the clear height for the same factor *Fa*. They compared the results with their experimental data.

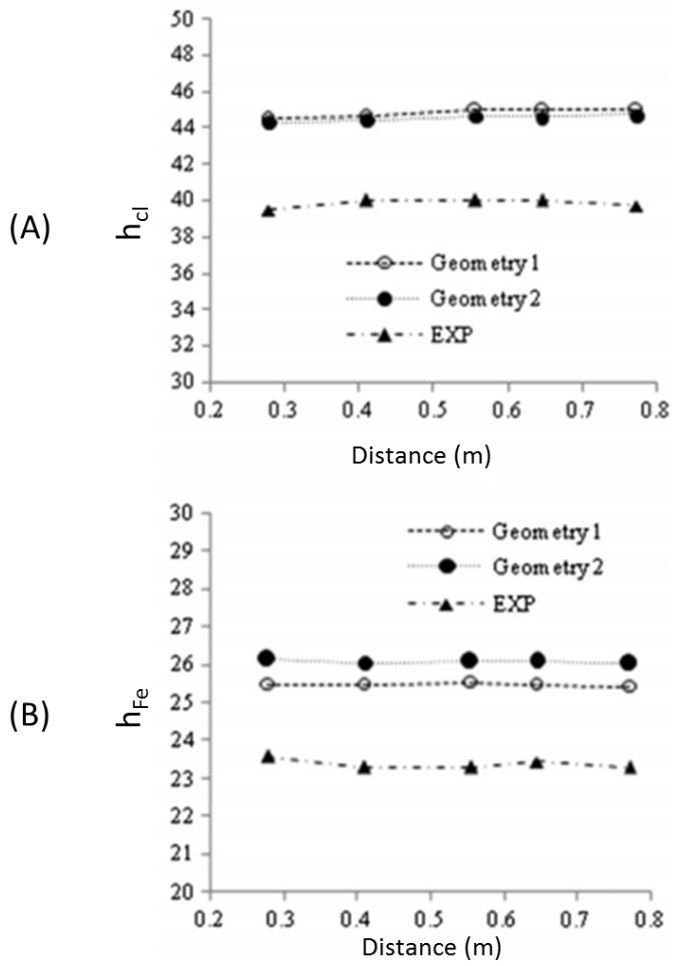

Figure 8- CFD simulations and experimental data for: (A) froth height, (B) clear liquid height at Fa=0.4 Pa $^{0.5}$. (Zarei, Hossein, & Rahimi, 2012)

3.1.3 **Interaction gas-liquid**

The difficulty resides in modelling the interaction gas liquid. The term of moment exchange (M_{GL}) in Eulerian model is described as a function of hydrodynamic forces exerted on the particles. For the particle in movement (Kolev, 2007) the term is the average of the hydrodynamic forces, expressed by equation 3-5:

$$\overrightarrow{M} = \left(\overrightarrow{M_D} + \overrightarrow{M_M} + \overrightarrow{M_{Tchen}} + \overrightarrow{M_H} + \overrightarrow{M_L} + \overrightarrow{M_T}\right) \qquad 3\text{-}5$$

It is possible to distinguish different forces: drag force ($\overrightarrow{M_D}$), Tchen force ($\overrightarrow{M_{Tchen}}$), Basset force ($\overrightarrow{M_T}$), lift force ($\overrightarrow{M_L}$), dispersion force ($\overrightarrow{M_H}$), and virtual mass ($\overrightarrow{M_M}$).

For the diphasic flow in trays and with high Reynolds number, the important forces are:

- Lift coefficient

- Virtual mass coefficient
- Drag coefficient (expression by (J.M.van Baten, 2000))

Several studies have been done in order to characterize theses forces. However the drag force is the most used force to characterize the "sum" of all forces. This force is express in the opposite way to the movement of flow. For one particle in the flow, the drag force is expressed as the following:

$$\overrightarrow{F_D} = -\frac{1}{2} C_D \rho_c \left|\overrightarrow{U_d} - \overrightarrow{U_c}\right| \left(\overrightarrow{U_d} - \overrightarrow{U_c}\right) A_d \qquad 3\text{-}6$$

With A_d being the surface project by the particle, C_D the drag coefficient, c for the continuous phase and d for dispersive phase.

The coefficient depends of hydrodynamic, the nature of the particles, the geometry form of the particles, the retention of dispersive phase, the turbulence, etc.

For bubble flow different studies have been done (Van Baten and Krishna, 2000, 2003; Li et al, 2009. Jiang et al, 2012; Zarei and al, 2012). The expression used for this work is the most used expression of C_D. Krishna et al (1999) proposes a law for the drag coefficient that was developed for bubble columns with high gas retention (up 45%). The drag coefficient is expressed as follows (equation 3-7) :

$$C_D = \frac{4}{3} \frac{\rho_L - \rho_G}{\rho_L} g d_G \frac{1}{V_{slip}^2} \qquad 3\text{-}7$$

Where the slip velocity, V_{slip} is the velocity estimated from the gas superficial velocity.

$$V_{slip} = \frac{U_s}{\alpha_G^{correlation}} \qquad 3\text{-}8$$

Where the correlation of volume fraction is given by Bennett et all 1983:

$$\alpha_G^{correlation} = \alpha_G^{Bennett} = 1 - e^{\left[-12.55 U_s \left(\sqrt{\frac{\rho_L - \rho_G}{\rho_L}}\right)^{0.91}\right]} \qquad 3\text{-}9$$

By substituting the momentum exchange due to drag force of Krishna et al (1999), it reduces to:

$$\overrightarrow{M_{GL}} = \alpha_L \alpha_G (\rho_L - \rho_G) g \frac{1}{\left(U_{G,a}/\alpha_L^{correlation}\right)^2 \alpha_L^{correlation}} \left(\overrightarrow{u_G} - \overrightarrow{u_L}\right) \left|\overrightarrow{u_G} - \overrightarrow{u_L}\right| \qquad 3\text{-}10$$

This formulation has been adopted for almost simulations for perforated trays (Krishna et al, 2000, 2003; Gesit et al. 2003) on valve trays (Li et al, 2009; Jian et al. 2012). But the expression for the gas retention retention α_G is different for all the works (see Figure 29 in attachments). The evolution of drag coefficient is depending on gas retention. Normally the

augmentation of superficial velocity, promotes the augmentation of the gas retention and the diminution of the drag coefficient.

3.1.4 **VOF model**

In order to qualify the interface gas-liquid, the VOF model is the most adequate. The approaches of VOF have been done by Asghar Alizadehdakhel et al, 2010 and Abid Akhtar et al, 2007 (they studied the effect of superficial gas velocities and gas distributors). Asghar Alizadehdakhel et al, 2010 studied the effect of valve weight on the hydrodynamic performance of the tray. The experiments and simulations are dedicated to a single valve device with three different grids. The VOF model is relatively simple to treat topologically changes of the interface. The sum of the volume fractions of all phases in each control volume is equal to one. The equations of conservation (equation 3-11) and momentum (equation 3-12) are:

Continuity:

$$\frac{d\rho\vec{u}}{dt}\nabla.\rho\vec{u} = 0 \qquad \textit{3-11}$$

Momentum:

$$\frac{\mathrm{du}}{\mathrm{dt}} + (\mathrm{uu}) = \frac{1}{\rho}[\nabla \mathrm{p} - \nabla(2\mu \mathrm{S})] + \frac{1}{\rho}\vec{F}_{\mathrm{SF}} \qquad \textit{3-12}$$

Where F_{SF} is the continuum surface force (CSF) vector and S is the deformation tensor given by:

$$\mathrm{S} = \frac{1}{2}\left(\nabla \mathrm{u} + [\nabla \mathrm{u}]^{\mathrm{T}}\right) \qquad \textit{3-13}$$

ρ is the density and μ the viscosity of the fluid depending on volume fraction of each phase. They are calculated by the following equations:

$$\rho = \alpha\rho_{\mathrm{G}} + (1-\alpha)\rho_{\mathrm{L}} \qquad \textit{3-14}$$

$$\mu = \frac{\alpha\rho_G\mu_G + (1-\alpha)\rho_L\mu_L}{\alpha\rho_G + (1-\alpha)\rho_L} \qquad \textit{3-15}$$

Where α is the air volume fraction in the cell. So the interface between gas and liquid was tracked by the volume fraction. The conservation of α can be represented by the interface mass balance:

$$\frac{\mathrm{d}\alpha}{\mathrm{dt}} + \mathrm{u}.\nabla\alpha = 0 \qquad \textit{3-16}$$

The interaction causes more contact between the phases upon the tray. Figure 9 shows counters of liquid phase volume fraction in the column. According to the figure, liquid flows downward from the liquid inlet. The gas goes upward from the tray's hole, hits the liquid and divides into small bubbles (Asghar Alizadehdakhel et al, 2010).

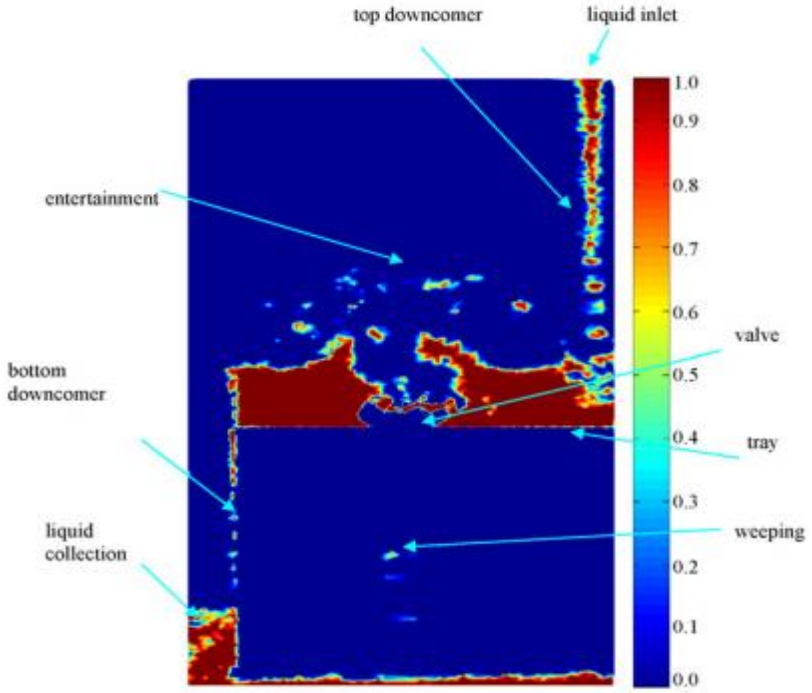

Figure 9- Contour plot of the liquid volume fraction in the column (Alizadehdakhel, Rahimi, & Alsairafi, 2010)

The pressure drop change gradually on the tray due to the liquid's weight except in the regions closer to the valves. This causes the air bubbles collapse and divert to lateral sides. A negative pressure in the downcomer can be explained by the pressure region created by the gravity. They compare their experimental and simulation results and both are in a good agreement.

4 Hydrodynamic Modelling

4.1 Model Geometry

Determining the model geometry was the first step towards solving the two-phase flow problem. The Gambit 2.3.6 program was used to create a geometry and mesh. This geometry tries to be a faithful copy as possible of the experimental set-up (see Figure 10).

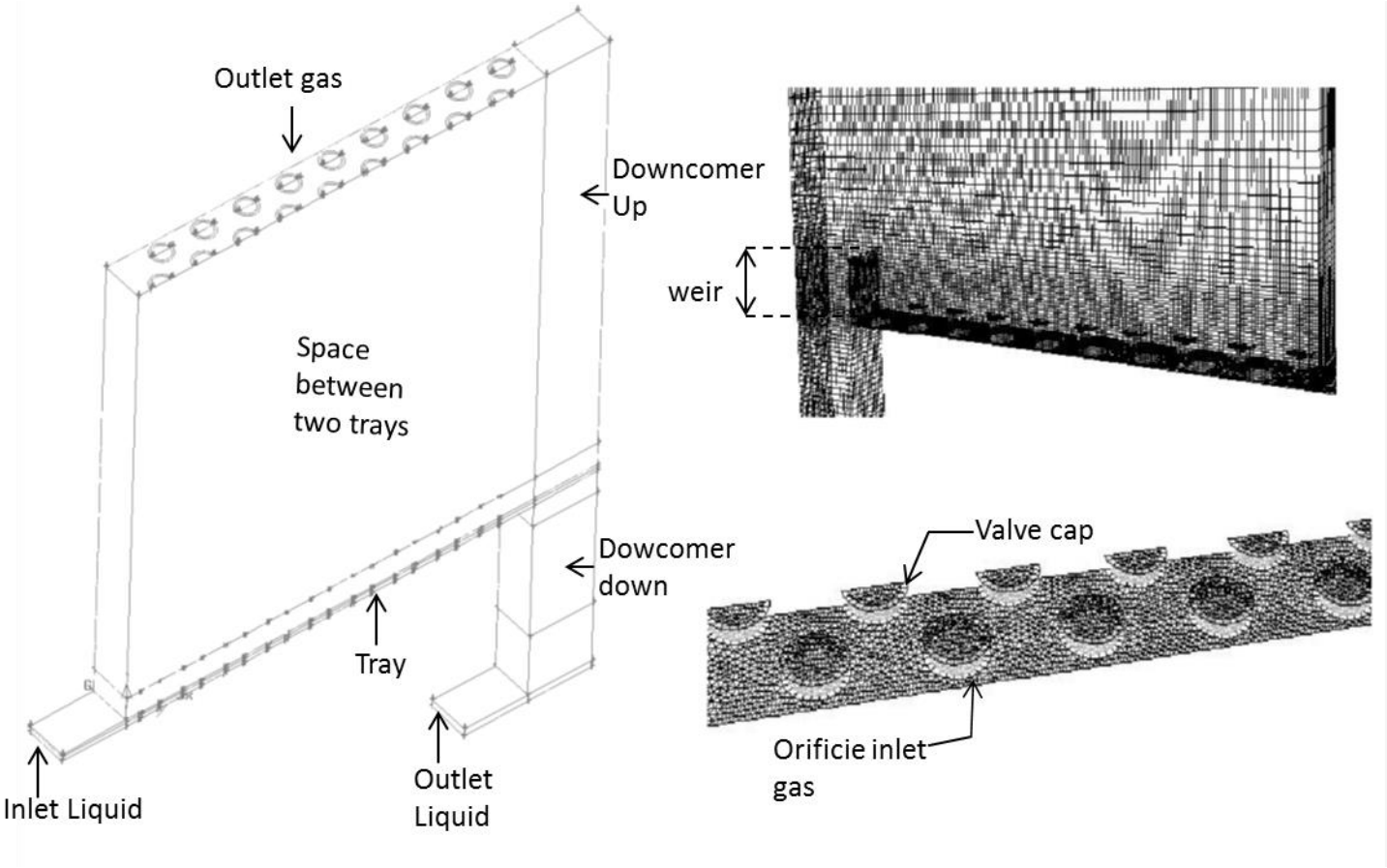

Figure 10-Scheme of the geometry

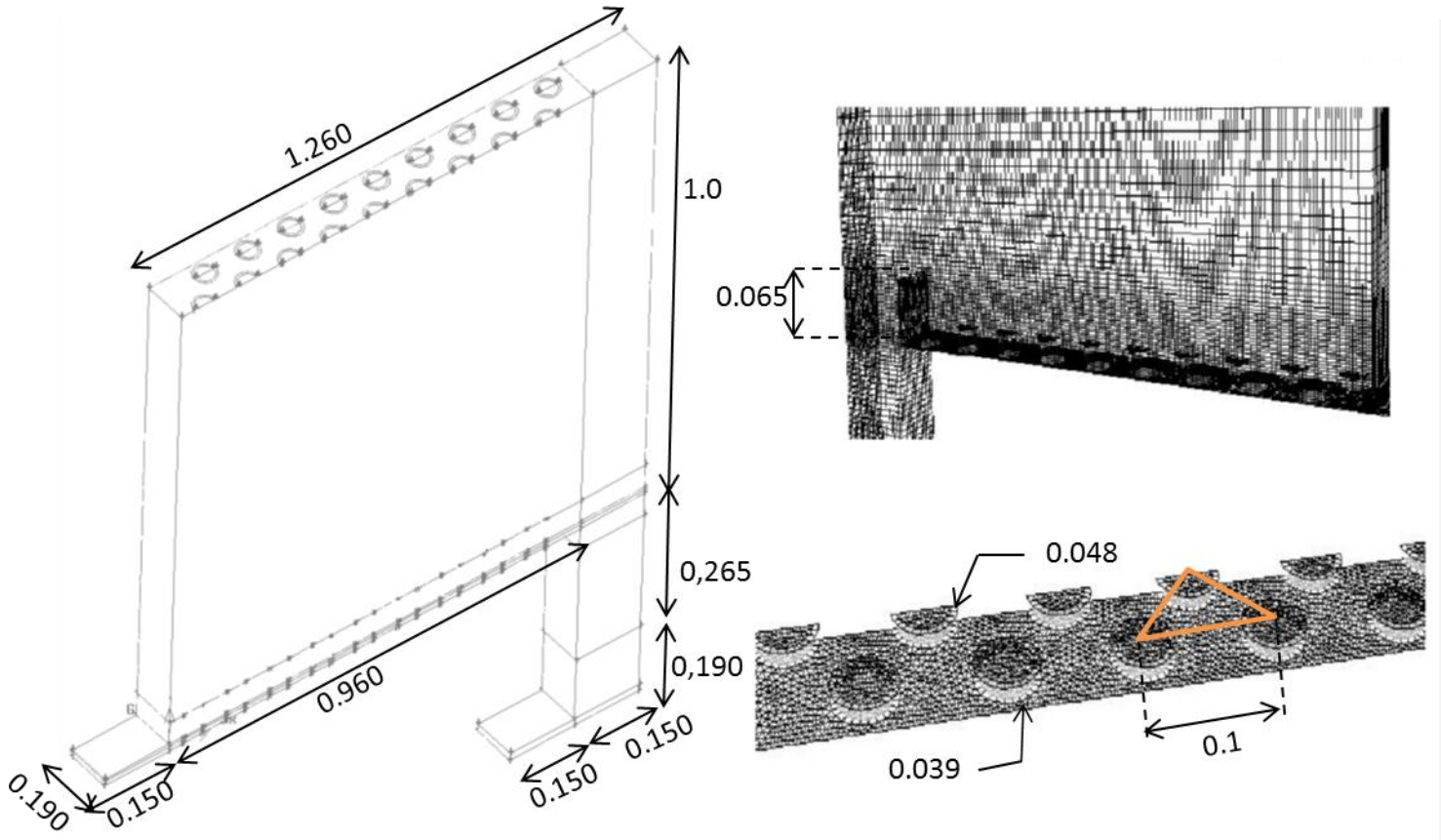

Figure 11- Dimensions of Geometry

The described of the flow path has already done in the chapter 2 of Context (Tray Technology).

4.1.1 **Meshing**

Determining a mesh was the second step towards solving the two-phase flow problem. In order to high-quality grids, all the faces with circular form adopt triangular element with a small mesh interval size for better accuracy. The other regions with rectangular form adopt a quadrangular element. The element for meshing the volume was specified as a hexahedron. A scheme of cooper was used to extrapolate the mesh of faces to volumes. This type of scheme seeps the mesh node patterns of specified “source” faces through the volume. Different levels of refinement are used according to the distance of section to the tray, the interval account is 10. The total cells are around 0.4 million. The grid was adapted by other work (Brahem, 2013), so the dependence of the grid does not test.

5 Hydrodynamic Modelling: Gas

5.1 Introduction

In this chapter is proposing the study of hydrodynamics of the gas in an absorption column equipped with valve trays. Simulations are compared with the experimental results and theoretical values. An introduction to the hydrodynamics is first proposed. Secondly conditions used for the simulations are presented. Finally the results are discussed.

5.1.1 Pressure Drop in gas-liquid configuration

The pressure drop for an absorption column is one of parameters used for scaling and operating the column. The total pressure drop is characterized by the sum of different pressures drop along the columns. We define two different pressure drop, represented in Figure 12: first the pressure drop due to the valve (Δp_{tray}) and second the pressure drop due to the emulsion created by the bubbling of the gas in the liquid layer above the tray ($\Delta p_{emulsion}$). Uniform pressure is assumed in horizontal control surface. Equation 5-1 represents the total pressure drop in the absorption column (for one stage):

$$\Delta p_{total} = \Delta p_{tray} + \Delta p_{emulsion} \qquad 5\text{-}1$$

$\Delta p_{emulsion}$ is the pressure drop mainly created by the weight of the emulsion above the tray. Δp_{tray} represents the pressure drop through the tray, can be expressed by two contributions : first the weight of valves and secondly by the pressure drop due to the restriction (gas passes through the orifices of the tray). Thus we can write equation 5-2 as:

$$\Delta p_{tray} = \Delta p_{weigth\ of\ valve} + \Delta p_{"restriction"} \qquad 5\text{-}2$$

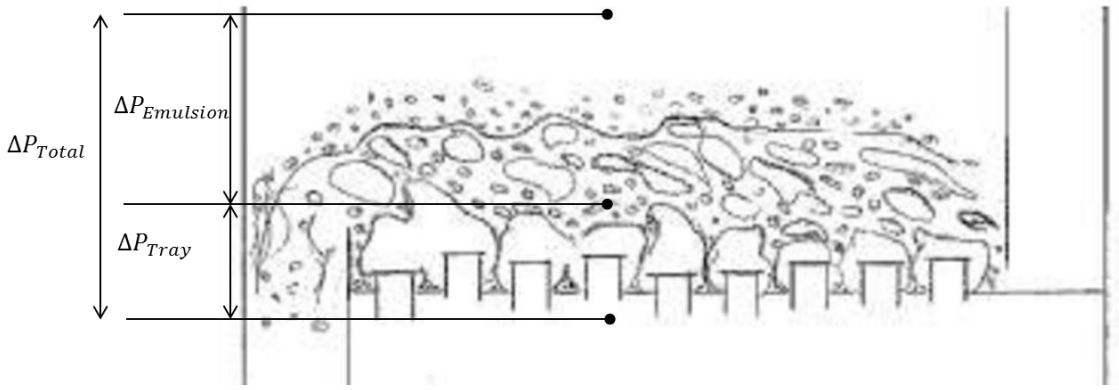

Figure 12-Pressure drop in two different zones

5.1.2 **Dry Pressure Drop**

In the literature generally the tray pressure drop (Δp_{tray}) with gas-liquid flow is as approximated by the dry pressure drop that is the pressure drop due to restriction and weight of valve with no liquid. With gas only and for perforated tray (no valve) the usual way to represent $\Delta p_{"retriction"}$ is, equation 5-3:

$$\Delta p_{\text{"restriction"}} = \frac{\xi \rho_G U_{G,h}^2}{2} \qquad 5\text{-}3$$

Where ρ_G is the gas density, $U^2_{G,h}$ the gas velocity at the restriction, and ξ the pressure loss coefficient which depends of the orifice geometry. The same equation can be used for the valve tray, with an adaptation for the different valve position. Figure 13 shows the three possible positions for the valve.

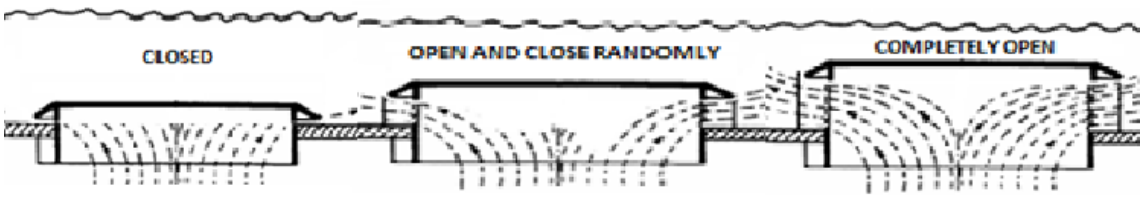

Figure 13- Different positions of the valve.

First Position: This case corresponds to a low gas flow rate, for which the valves are closed, the flow rate is not sufficient to contradict the weight of the valves.

Second Position: The pressure under the valves is sufficient to cause them begin to lift. The valves open and close randomly to accommodate the extra gas flow while the pressure drop remains approximately constant. By increasing the gas flow rate the area available for the flow increases so the velocity through the orifice remains almost constant and so the pressure.

Third Position: The flow rate is sufficient to completely open the valves and the pressure drop increases with the velocity. For this case $S\ (area)$ is constant, like in the first position.

Figure 14 is an example for dry pressure drop in valve trays related with the velocity in the hole.

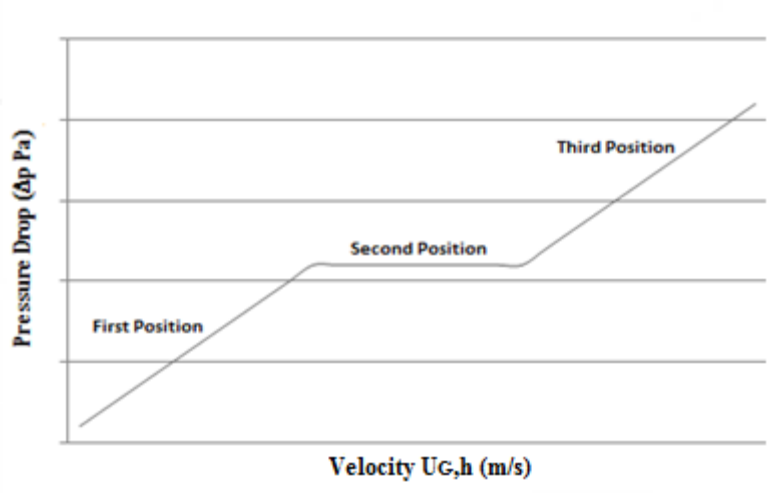

Figure 14- Dry tray pressure drop for a valve tray

There are many correlations available in the literature for $\Delta p_{"restriction"}$ Pinczewski et Fell (1975) studied three different perforated trays and propose the following expression:

$$\Delta p = 1{,}3\rho_G \frac{U_{G,h}{}^2}{2}\left[0{,}4\left(1{,}25 - \frac{A_h}{A_a}\right) + \left(1 - \frac{A_h}{A_a}\right)^2\right] \qquad 5\text{-}4$$

Where $\frac{A_h}{A_a}$ is the ratio between perforated surface and active area, active area represents all the surface of tray and perforated surface is the orifices where the gas passes, $U_{G,h}$ is the velocity of gas in the holes and ρ_G the gas density. For a large range of velocity the three zones described for the valve trays are observed. However the dependency of velocity square for the third zone does not always verify.

5.2 Experimental Results

The experimental works have been done during the thesis of Rim Brahem (Brahem, 2013). In experiment the measures of pressure drop were made with manometers, previously installed. Figure 15 represents the experimental results obtained over a wide range of gas velocity that is for the three different valves positions. In the graphic is easy to see the three different zones (positions of valves). For the theoretical values in the graphic was represented the third section.

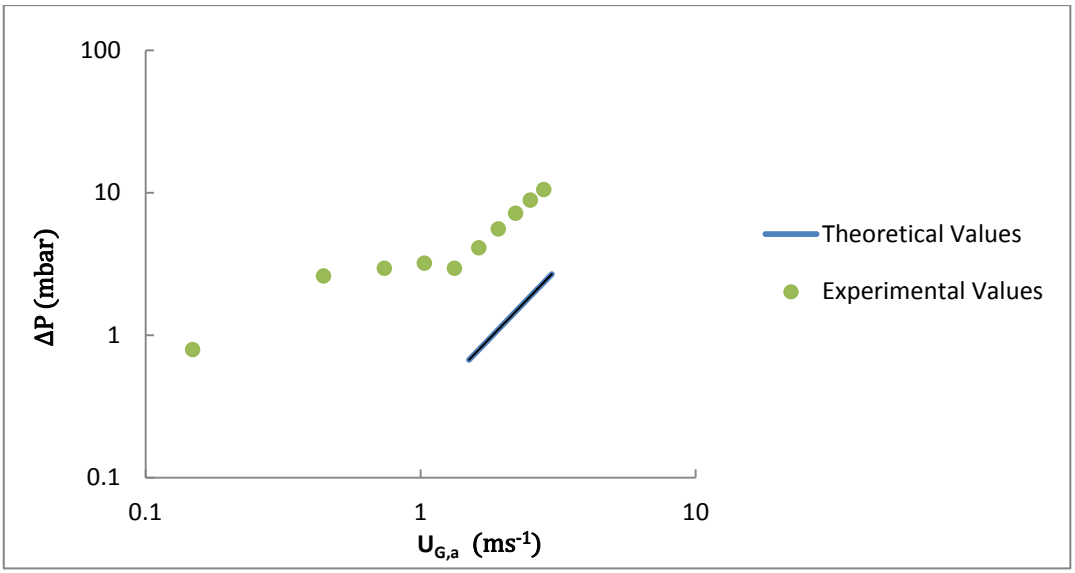

Figure 15- Experimental and theoretical values of absorption column

Theoretically, for valve completely opened, the pressure drop increases with the square of the velocity in the holes. Experimental results show a dependency closer to 1.7 for the third zone instead of 2. This value is equal to the one presented in the literature.

According to the experimental values a correlation for the third experimental zone was proposed (equation 5-5):

$$\Delta P_{\text{"restriction"}} = 1.5 Fa^{1.7} \qquad 5\text{-}5$$

The relative error for this correlation is 1.5 %.

Where Fa is the kinetic factor of gas and is equal to:

$$Fa = \sqrt{\rho} U_{G,a} \qquad 5\text{-}6$$

5.3 CFD Simulation

The simulations were carried out with ANSYS Fluent 15.0.0. For this work we are only interested in the third position, when the valves are completely open. The simulations with the valves open and close randomly is very complex and carried out an exhaustive study.

5.3.1.1 Model geometry

Determining the model geometry was the first step towards solving the gas flow problem. The specifications for the geometry were already presented in chapter 3 (3.1 Model Geometry).

5.3.1.2 Solution of model

The solver was considered to be a Pressure-Based solver which used the equations of continuity. The time was specified as Steady State. Other specifications had to be made related to the boundary conditions, such as the inlet and the outlet of liquid was a wall (see

Figure 16) In the case of valve tray with the gas flow rate only, the K-ε model was thought suitable. The material for the single phase simulation was air.

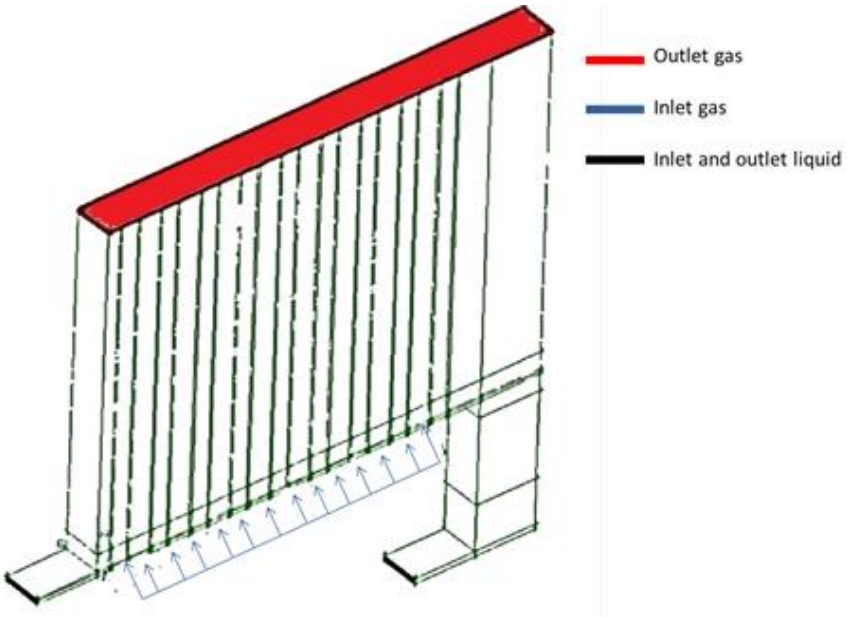

Figure 16- Sketch of Boundary Conditions

The inlet boundary conditions were set up was a velocity inlet, with a uniform distribution of *z* velocity component. The outlet conditions were set up by pressure outlet boundary (constant pressure in the outlet plane). The rest were defined like wall, interior or symmetry. The next table presents the summary of different conditions used for the simulations.

Table 3- Conditions for the CFD simulation

<table>
<tr><td>Models</td><td colspan="6">Standard K-epsilon</td></tr>
<tr><td rowspan="2">Boundary Conditions</td><td>Inlet Liquid</td><td>Inlet Gas</td><td>Outlet Liquid</td><td>Outlet Gas</td><td rowspan="2"></td><td rowspan="2"></td></tr>
<tr><td rowspan="5">Closed</td><td>Velocity Inlet $U_{G,a}$</td><td rowspan="5">Closed</td><td rowspan="5">Pressure Outlet</td></tr>
<tr><td>4,94 ms^{-1}</td></tr>
<tr><td>5,80 ms^{-1}</td></tr>
<tr><td>11,60 ms^{-1}</td></tr>
<tr><td>23,22 ms^{-1}</td></tr>
<tr><td rowspan="4">Solvers</td><td>Schema</td><td>Gradient</td><td>Pressure</td><td>Momentum</td><td>Turbulent Kinetic Energy</td><td>Turbulent Energy Dissipation Rate</td></tr>
<tr><td>Simple</td><td rowspan="3">Least Squares Cell Based</td><td rowspan="3">Second Order</td><td>First Order Upwind</td><td rowspan="3">First Order Upwind</td><td rowspan="3">First Order Upwind</td></tr>
<tr><td>Simple</td><td>Second Order Upwind</td></tr>
<tr><td>SimpleC</td><td>Second Order Upwind</td></tr>
<tr><td>Monitors</td><td colspan="6">Area Average: Pressure in the inlet gas and outlet gas.</td></tr>
<tr><td>Value Tested</td><td colspan="6">Pressure drop for different velocities</td></tr>
</table>

The Solution Methods to solve the coupling between the velocity and pressure were changed for the different simulations. By selecting specific Monitors, the pressure could be monitored during solving, to show the average pressure at the inlet and outlet throughout the solution process.

The resulting graph of inlet and outlet pressure was used to monitor if the problem was close to a final solution. The Surface Monitor allowed for a visual assessment of whether the current set of iterations would result in a viable solution or if additional iterations were required.

5.4 Results

Different simulations were tested as shown in Table 1. As expected the results of the simulations will be between the theoretical and the experimental values. Figure 5 represent the results of simulations, experimental and theoretical values.

The simulation results are close to the experimental results. This was expected because theoretical equation is for perforated trays and experimental results are for valve trays like as simulation results.

During the simulations some differences were appeared related to response time need to converge and stabilized. Simulation 1 (Simple First Order upwind) was much faster. Simulation 2 (Simple Second Order) has better residuals (less residual) and simulation 3 (SimpleC Second Order upwind) was as simulations 2. The value of residuals (for the convergence) was considered $1x10^{-4}$.

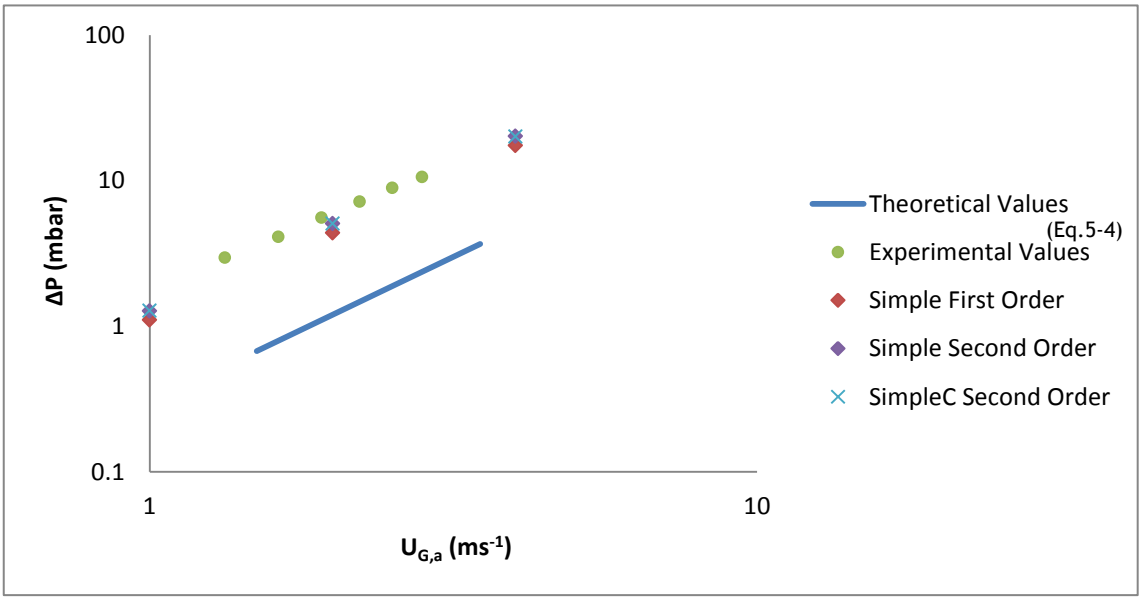

Figure 17- CFD results for the three simulations

Figure 6 represent the velocity magnitude in the plan *x*-*z*. The velocity increases when the gas enters the valve and come to maximum at the lateral outlet of valve, then decreases with the valve cap. After the gas ascend until the pressure outlet.

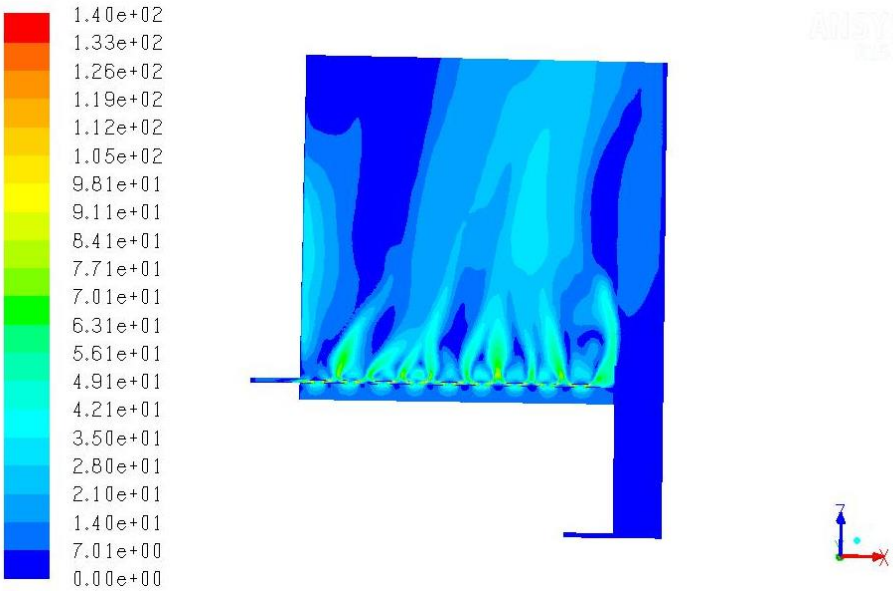

Figure 18- CFD Fluent: Velocity magnitude in plan x-z

The results are in a good agreement with experimental values. However the simulations do not present a dependence of 1.7, but 2 ($\Delta P = 1.5Fa^2$).

One reason for all these results is the fact of the theoretical values does not have valves, so the pressure drop created by them doesn't exist.

Other reason is because the experimental values of pressure drop are equal to the $\Delta \boldsymbol{p_{tray}}$ (equation 1-2). So the pressure drop created by *'restriction'* and the pressure drop created by the weight of the valves.

Finally the simulations have the pressure drop created by the *'restriction'* and also a pressure drop created by the impact of the flow with the valve cap (wall). This makes the simulations results to be between the theoretical and experimental values.

The simulations provide clear knowledge of the gas flow, which is helpful for the two phase's simulations, to describe the pressure drop for the two phases.

6 Hydrodynamic Modelling: Gas-Liquid

6.1 Introduction

In this chapter is proposed the study of hydrodynamics and interaction of the gas-liquid in an absorption column equipped with valve trays. An introduction to the hydrodynamics parameters and interaction gas-liquid is first proposed. Secondly simulations are compared with the experimental and theoretical values. The conditions used for the simulations are then presented. Last results are discussed.

6.2 Eulerian-Eulerian model

6.2.1 Emulsion Height, Clear liquid height and Liquid Retention

The emulsion height (h_{Fe}) is the height of the bed (gas-liquid) above the tray.

The clear liquid height (h_{cl}) represents the weight of liquid in the tray, is the height of liquid without gas. This height is related with the emulsion height, by the following equation 6-1:

$$h_{cl} = \alpha_L h_{Fe} \qquad 6\text{-}1$$

Where α_L is the liquid retention. Figure 19 is a scheme where the hydrodynamic parameters are represented. The pressure drop was treated in the chapter 4.

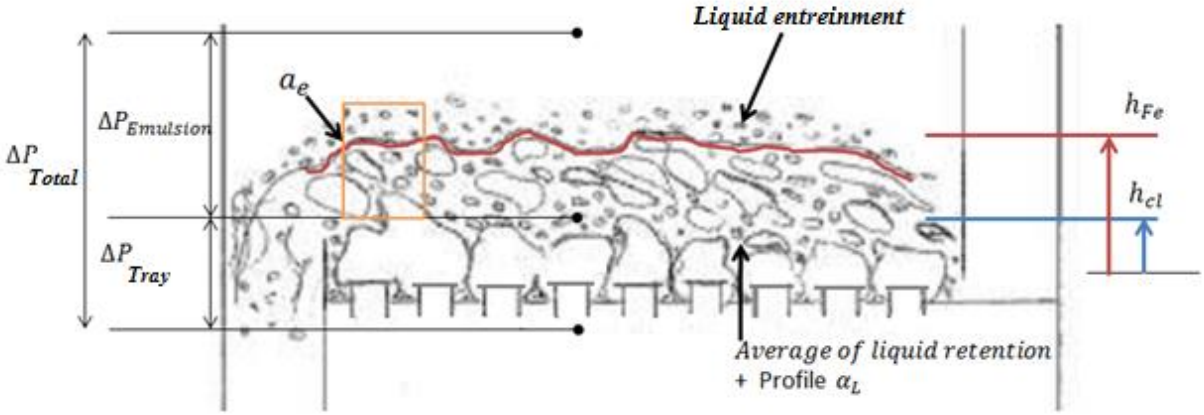

Figure 19- Represent all the hydrodynamic variables. These variables were referenced in the literature. Pressure drops, clear liquid height (h_{cl}), emulsion height (h_{Fe}), liquid retention (a_L) liquid entrainment and interfacial exchange area (a_e).

The correlations for liquid retention have been introduced in chapter 3 (3.12-Interaction gas-liquid). As already written, different correlations exist to calculate the α_L (Figure 29 in attachments). Bennett et al. (1983) correlation is the most used.

Also Benett et all. propose an expression to calculate the clear liquid height:

$$h_{cl} = \alpha_L^{average}\left[h_w + C\left(\frac{Q_L}{W\alpha_L^{average}}\right)^{0.67}\right] \qquad 6\text{-}2$$

$$C = 0.50 + 0.438e^{-1.37h_w} \qquad 6\text{-}3$$

Where $\alpha_L^{average}$ is determined by equation 3-9, h_w is the weir height; $\frac{Q_L}{W}$ is the liquid weir load. These are empirical equation, and further are used to compare with the simulation results.

6.3 CFD Simulation

6.3.1 Drag Force: Implementation in Fluent

The Fluent commercial code provides the ability to model the interaction term between the two phases by a term exchange of momentum. The momentum exchange is formulated via a drag force, an added mass force, a lift force and/or via the effect of interfacial tension.

As written in Chapter 3 (Interphase gas-liquid), only the drag force is considered in this work to describe the momentum exchange. This can be customized by using a UDF (User Defined Function). The general form of the drag force as expressed in the code:

$$\overrightarrow{M_D} = -K_{dc}\left(\overrightarrow{U_d} - \overrightarrow{U_c}\right) \qquad 6\text{-}4$$

Where $\left(\overrightarrow{U_d} - \overrightarrow{U_c}\right)$ is the slip velocity between the disperse phase and continuous phase. K_{dc} is an adjustable coefficient in the fluent.

With the right shape for this coefficient it is possible to impose a specific law of drag force. The proposed equation 6-5 by Van Baten et al (1999) and originally developed for bubble columns (Krishna et al, 1999) is used in numerical simulation of perforated trays and valves, in part of this work the expression is tested in part of this work.

As a reminder, the momentum exchange with the term of drag force is expressed:

$$\overrightarrow{M_{GL}} = \alpha_L\alpha_G(\rho_L - \rho_G)g\frac{1}{\left(U_{G,a}/\alpha_L^{correlation}\right)^2\alpha_L^{correlation}}(\overrightarrow{u_G} - \overrightarrow{u_L})|\overrightarrow{u_G} - \overrightarrow{u_L}| \qquad 6\text{-}5$$

In the Fluent code K_{dc} is expressed by:

$$K_{dc} = \alpha_L \alpha_G (\rho_L - \rho_G) g \frac{1}{\left(U_{G,a}/\alpha_L^{correlation}\right)^2 \alpha_L^{correlation}} \qquad 6\text{-}6$$

6.3.2 CFD results

A previous simulation has been done, for a different geometry. These results are compared with the experimental results and the theoretical results of Van Batten. The boundary conditions for these simulations are the following:

- Inlet gas/Inlet liquid: Uniform Velocity $V_{in,L}/V_{in,G}$
- Outlet gas: Atmospheric Pressure, P_0;
- Outlet liquid : two conditions
  - $V_{out,L} = -V_{in,L}$
  - Hydrostatic pressure, calculated by the experimental results
  - $P_{hydro} = P_0 + \Delta P_{valve} + \Delta P_{emulsion} + \Delta P_L$, Where $\Delta P_L = \rho_L V_{in,L}^2$

Symmetric plan

Figure 20 represent a comparison between the experimental results and simulations (based on the correlations of Van Batten) for the three hydrodynamic parameters.

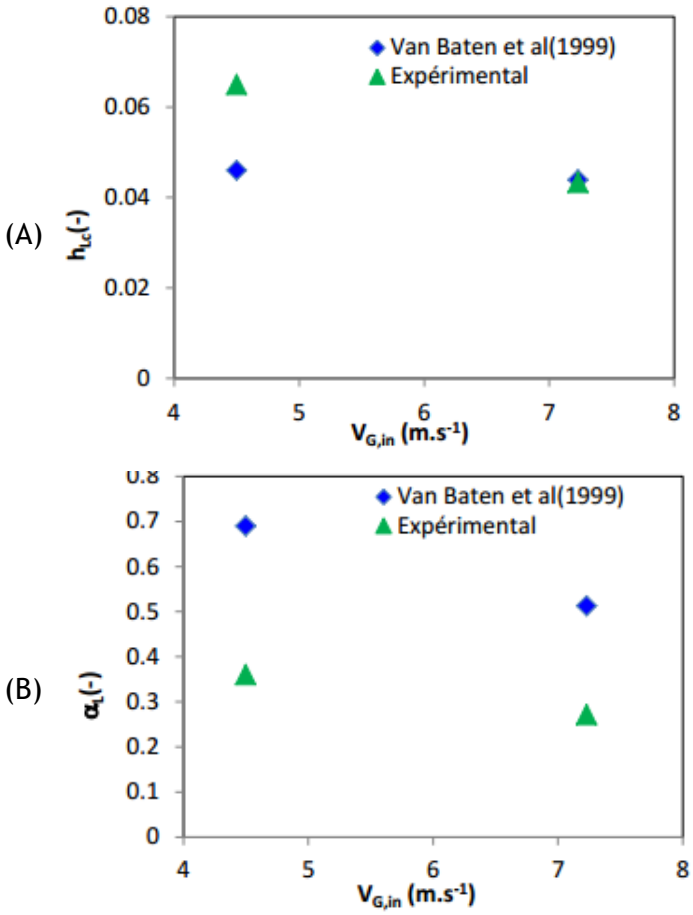

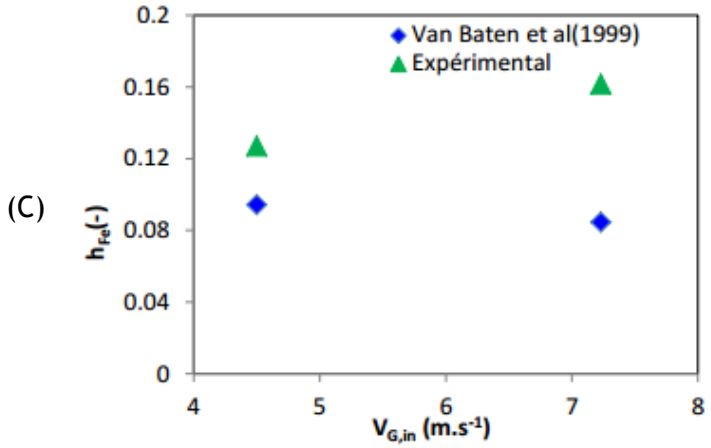

Figure 20-Comparation of the simulations results (implemented with Van Baten et al. (1999) low) and experimental results for two different velocities, (A)-Liquid retention, (B)-Clear liquid height and (C)-Emulsion height.

The most important results are the retention of liquid. Other law for liquid retention possibly gives better results. The theoretical values just take in account the drag force which is a simple way to represent the reality.

Images of the simulations are presented in the Figure 21. This corresponds to a velocity inlet in the valves of gas equals to 7.23 ms^{-1} (*Fa*=1.4 Pa$^{0.5}$). These results show the behaviour of the flow and the influence of valves in the distribution of two phases in the tray.

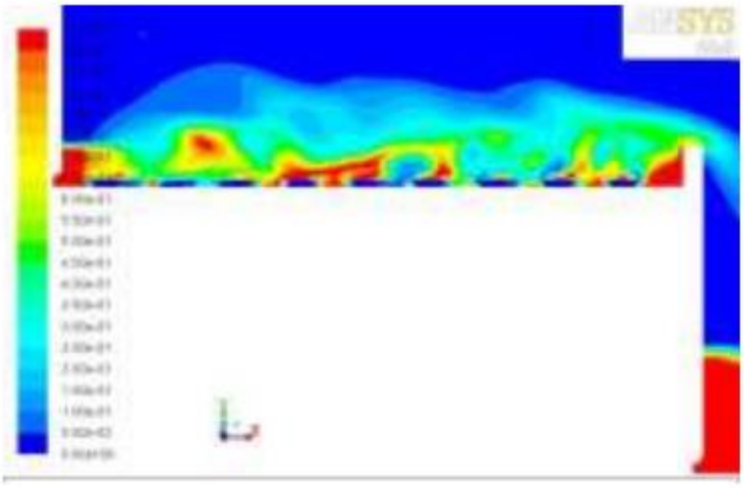

Figure 21- Representation of liquid retention of the symmetry plan of the column.

Simulations tested with different values for drag force constant, shows an important rate of entrainment of liquid in the gas. Because of this problem a propose modification of the drag correlation have been done (Brahem, 2013). The idea is to annulet the interaction term for the high retentions of gas. This makes the liquid separate of the gas for high distances of tray. The expression proposed is:

$$\overrightarrow{M_D} = K' C \rho_L \frac{\alpha_G}{h_{max}} \left|\overrightarrow{U_G} - \overrightarrow{U_L}\right| \left(\overrightarrow{U_G} - \overrightarrow{U_L}\right) \qquad 6\text{-}7$$

In order to eliminate the term of interaction a value for α_G is fixed and is called α_s (this term remove the interaction) .To avoid discontinuity the diminution of the drag in function of gas retention is controlled by adding a decreasing exponential.

$$\text{If } \alpha_G < \alpha_s \qquad K' = 1 \qquad 6\text{-}8$$

$$\text{If } \alpha_G > \alpha_s \qquad K' = \exp\left[\beta\left(\frac{\alpha_s - \alpha_G}{1+\varepsilon-\alpha_G}\right)\right] \qquad 6\text{-}9$$

Where β is a decreasing coefficient, ε is a constant (10^{-6}).

Whit this expression some problems related with entrainment of liquid was solved, but in the other hand problems with divergence remains.

6.3.3 **Model geometry**

The specifications of geometry were already presented in the chapter 3. However some differences in the geometry were made in order to find more suitable one. Three geometries were tested. The same dimensions and the same mesh are used for the three geometries (Chapter 3). Geometry one have a volume below the tray where the gas enters. This volume promotes the uniformed entrains of the gas velocity. The second geometry is different, the volume related with the inlet gas (before the tray) was removed. In this case the gas velocity inlet is imposed directly in the holes of valves (tray orifices). Last the geometry three, the difference in this geometry is the dowcomer down/up and liquid exit they were removed.Figure 22 represents the three geometries.

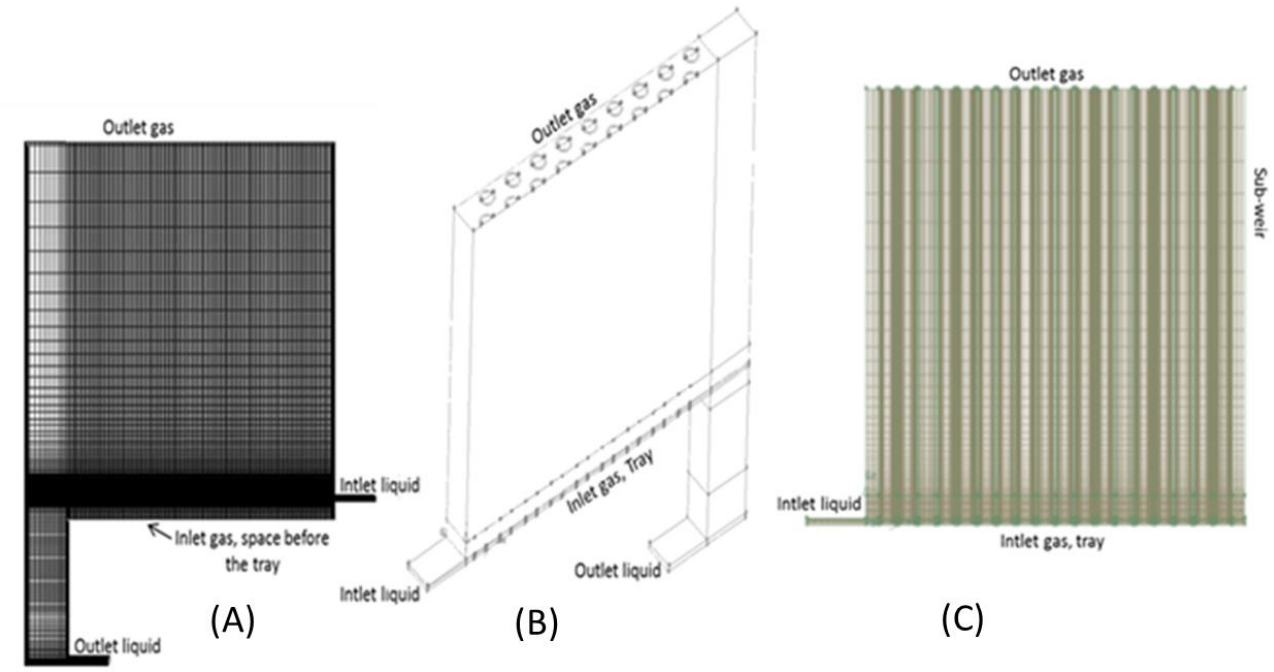

Figure 22-Different geometries used in this work. (A)- First geometry; (B) - Second geometry without the space before the tray and (C)-Third geometry without the downcomers and liquid outlet.

The first or second geometry are the most adequate geometries. Because these geometries were the faithful copy as possible of the experimental set-up. The third geometry as tested because is more simple than the other and take to less time to simulate, but does not give a good solution.

6.3.4 **Boundary Conditions**

Different boundary conditions have also been tested. The monitors, inlet velocities and the solutions methods do not change for all geometries. The velocities are 7.23 ms^{-1} in the hole of the valve for the gas and 0.642 ms^{-1} for inlet liquid.

6.3.4.1 Gas

Different boundary conditions were tested for the three geometries. The same diameter for the gas bubbles was used (0.009 mm) For the first simulation, with first geometry, the boundary conditions tested for the gas were pressure outlet and velocity inlet (see Figure 23).

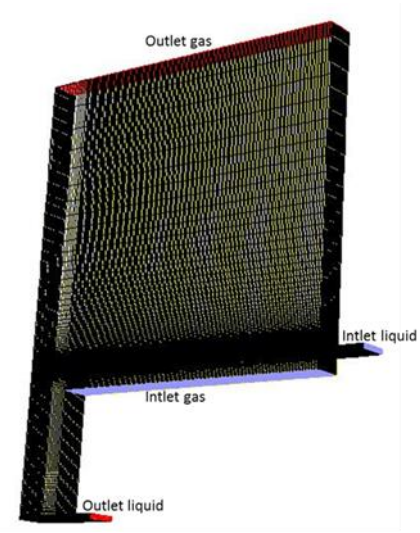

Figure 23- Boundary conditions of gas for the first geometry

The same conditions used for the first simulation were tested for the second geometry (pressure outlet and velocity inlet for gas) and also a degassing condition (for the outlet gas) was tested. Other outlet was tested; with second geometry. The simulation is like simulation 2-1 with gas outlet as pressure outlet, but the outlet gas is not the entire surface see Figure 24(A). In this case the outlet gas is only the holes (orifices) like represented by the Figure 24 (B).

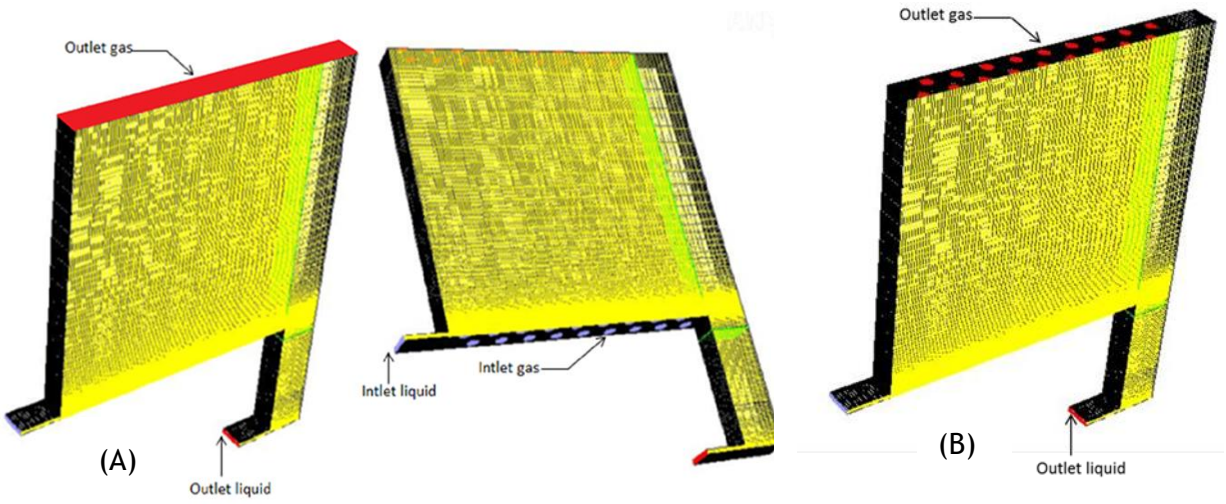

Figure 24- Boundary conditions of gas for the second geometry. (A) - Entire surface and (B) - orifices

For the third geometry the same conditions were tested, pressure outlet for the gas outlet, velocity inlet for gas. After the position of outlet gas was changed to the wall above the weir. For this change different boundary conditions was tested like as: pressure outlet, outflow, degassing. (See Figure 25)

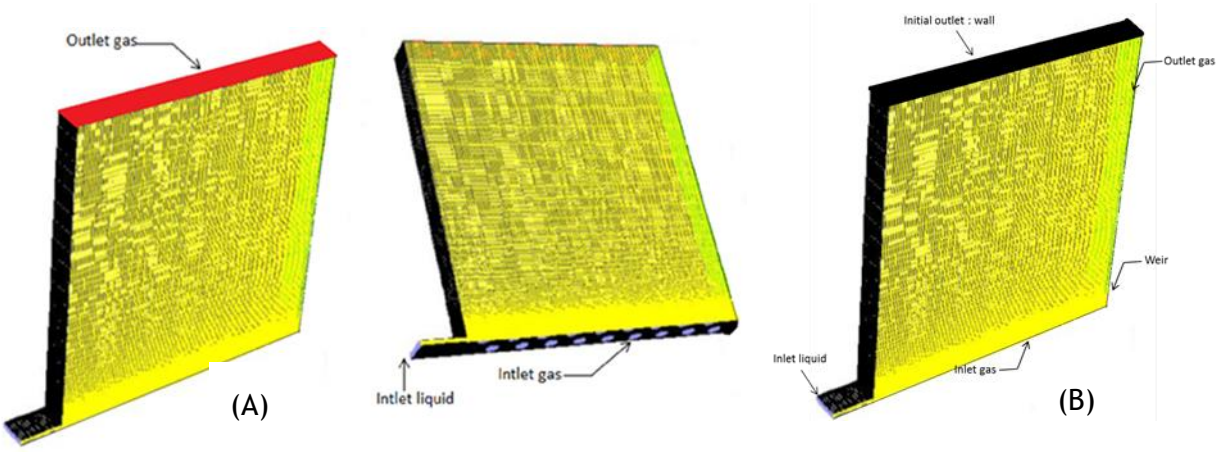

Figure 25- Boundary conditions of the gas for the third geometry. (A) -First outlet gas and (B) - Second outlet, with exit gas the wall above the weir.

With simulation of Rim Brahem (files cas and dat), the second geometry was replaced and tested. For this simulation only the condition of degassing was tested in the outlet gas.

Until now the most adequate representation of the experimental set-up is the second geometry with the exit gas as orifices, Figure 24 (B). The orifices are an entry of gas for the tray above. For this geometry the most adequate boundary conditions of gas is velocity inlet and pressure outlet (atmospheric pressure). These conditions are suitable because are near to the reality.

6.3.4.2 Liquid

For the liquid boundary conditions the velocity inlet was used for all simulations. Relatively to the boundary condition for the liquid exit the most used was pressure outlet (to ensure that the gas goes to his exit).Another condition tested was velocity outlet but the gas goes to the exit of liquid. Some simulations started with the outlet liquid closed, but after the exit was opened.

So the geometry 2 with orifices as outlet gas, with boundary condition for the gas and liquid, pressure outlet and velocity inlet is the best solution.

6.3.5 **Initialization**

Relatively to initialization the most important thing to do is trying to make an initialization near to the final solution. The first approach was an initialization with the velocity of water entraining in the different directions (along the path) and also with the velocity of gas and with the volume fraction of gas in the different sections (downcomers up/down, tray, space between the two trays, etc). However the velocity is not so important like the volume fraction, so the initialization was done with volume fraction of gas (see Table 4)

Table 4- Patch (volume fraction of gas) in different volumes

Volumes of Geometry	Patch (Volume fraction of gas)
Inlet liquid	0
Inlet liquid	1
Outlet liquid	0
Outlet gas	1
Tray	0,7
Dowcomer up	
Space between tray and outlet gas	
Dowcomer down	0

6.3.6 Interaction gas-liquid

Some simulations were tested without interaction, other simulation with interactions of fluent like symmetric and a schiller-naumann. However the final interaction should be as user-defined (Krishna et all 1999). The solution without interaction is not a good one because does not represent the reality. For beginning the symmetric or schiller-naumann interactions are a better solution. After that UDF should be used.

6.3.7 Discretization model

The solver was considered to be a Pressure-Based solver which used the equations of continuity and momentum. The time was specified as transient. The model used is Eulerian-Eulerian for the multiphase and standard K-ε for the turbulence.

6.4 Results

A lot of combinations were done with the parameters presented above. The solutions with boundary condition degassing do not work for this case. The degassing condition is appropriate for bubble columns, when the phase near to the boundary is the liquid phase and not the gas phase.

Problems related with divergence in AMG solver or related with a high pressure in the outlet gas and low pressure in the outlet liquid or with the gas phase passes through the liquid outlet, were detected for some simulations.

So the solution is the second geometry with the holes as outlet gas. The boundary conditions are pressure outlet for gas and liquid and velocity inlet for gas and liquid. For beginning the schiller-naumann interaction is adequate.

Until this time the solution is not finished, but seen to the convergence. The solution is running approximately during three weeks. But until tod the solutions was not yet stable. The time step was 2×10^{-5} s. The expected is that the solution is near to the simulation values of Rim Braham, relatedly to the parameters like h_{cl} and h_{Fe}. Figure 26 represents the contours of volume fraction of gas and the vectors of velocity.

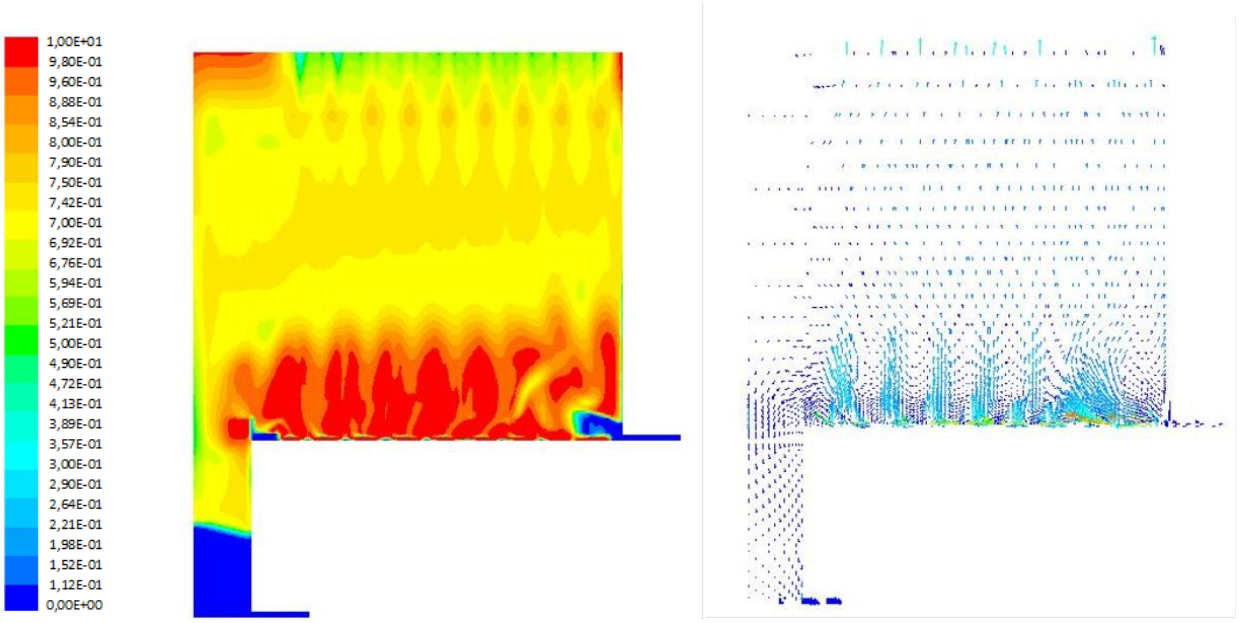

Figure 26- Contours of volume fraction of gas and the vectors of velocity.

The Figure 26 shows the water in the beginning of the tray, this is normal because it only passed pass 6.24×10^{-1} seconds. Relatively to mass flow rate, some water pass through the exit gas. However goes to the convergence. The pressure in exit water is bigger than in exit air like expected.

As expected the velocity of gas is higher in the inlet and in the exit of gas. In the zone of valves it is normal to have some recirculation of gas. It is impossible now to see the liquid retention or the clear liquid height. However is supposed that the liquid retention is higher near to the inlet liquid, near to the walls column and above the valve cap.

6.5 VOF model

6.5.1 CFD Simulation

A theoretical introduction was already done in chapter 3. The same procedure as Eulerian-Eulerian model will be applied for the VOF model. However for the reasons presented before

the VOF models need a different geometry, with different initial conditions. The results of this simulation will be presented and discussed.

6.5.2 Model geometry

The geometry for the VOF model is a piece of the original geometry (presented in chapter 3), this geometry represent only one valve of the tray. The mesh is the same like as Eulerian-Eulerian simulation with an evident difference in the number of cells (53600 for the VOF model).

6.5.3 Solution of model

For the VOF simulation was considered a Pressure-Based solver which used the equations of continuity and momentum. The time was specified as transient. The solutions methods are the same, also the monitors and the patch. A surface tension was applied for two simulation and also a different boundary conditions. The *K-ε* model was thought suitable.

For the simulation the liquid is stagnated, the gas enters through the valve with a velocity inlet 7.23 ms^{-1}. The outlet conditions were set up by pressure outlet. The tray was defined like wall and the limits of the geometry are defined as symmetry. Initially, the outlet gas was defined as the entire of surface. Afterward, the outlet was changed to the hole. Figure 27 represent all the boundary conditions.

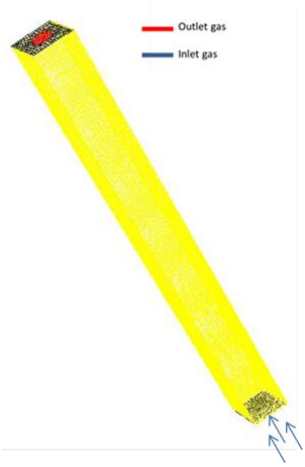

Figure 27- Sketch of Boundary Conditions

The next table presents the summary of the conditions, used for the simulation. In the VOF simulation the time step has to be smaller compared with the simulation for Euler-Euler. If not the global courant number is greater than 250, this makes the velocity diverge.

Table 5- Conditions for the CFD simulation

Models	Standard K-epsilon					
Boundary Conditions	Height Liquid	Inlet Gas	Outlet Liquid	Outlet Gas		
	0,265 m	Velocity Inlet $U_{G,a}$ 4,94 ms^{-1}	--	Pressure Outlet		
Solvers	Schema	Gradient	Pressure	Momentum	Volume Fraction	Transient Formulation
	Fraction Step	Least Squares Cell Based	PRESTO	Second Order Upwind	Compressive	First Order Implicit
Monitors	Mass flow rate of gas inlet and outlet					
Value Tested	Interaction of gas liquid					

6.5.4 **Results**

Until now the simulation goes in a good direction, but moves to the convergence. Figure 28 (A) shows the beginning of simulation, where is easier to see the patch, water in the bottom and air until the exit. After that, the gas begins to create its path and the water is entrained with the gas. However some of the water goes down, and some goes until the exit gas. Figure (A), (B), (C) show the evolution of the contour of water.

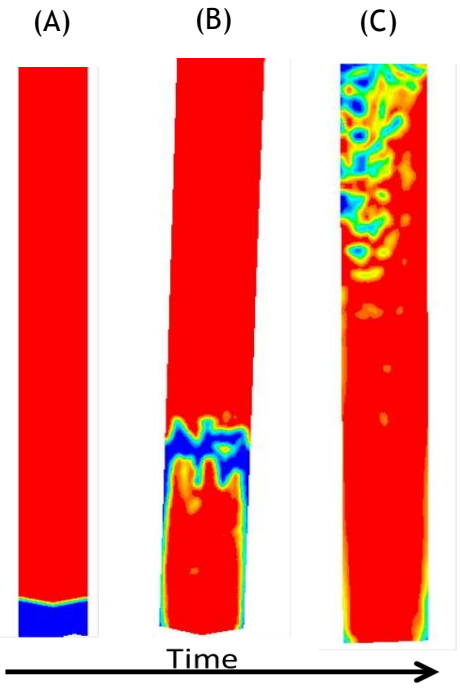

Figure 28- Contour of air for the VOF model

In the end it is expected that, the gas continues made its path, when finished and established, the water can come down to the initial position. In the final of simulation the contours will be show:

- Some entrainment of water in the gas;
- Water close to the symmetric wall, because the gas is pushed it against the walls and kept it there.

After that if the results are not goods the same simulations can be realized, with an inlet and outlet of water and impose a velocity inlet and a pressure drop for the outlet water.

7 Conclusions and Final Overview

CFD simulations were applied to the particular case of valve trays. Simulation studies took too much time, detail and thorough. The results of the pressure drop for the simulation with gas only are in good agreement with the experimental and theoretical values.

For the simulation with two phases and with an Eulerian-Eulerian model, the study and improvement of geometry and boundary conditions was made to find a good combination between each other. Three geometries were tested for different conditions. The conditions tested are: boundary conditions, interaction between the two phases and different initializations.

The best solution proposed is the geometry where the exit of gas is the holes of the valves for the “tray above”. The boundary conditions are pressure outlet for gas and liquid and velocity inlet for gas and liquid. The schiller-naumann interaction was used for the first approach. However the solution did not converge yet. The solution is in good agreement with what was expected such as the pressure in the outlet liquid to be higher than the pressure of outlet gas.

After that with first simulation, the UDF of Krishna et al 1999 should be tested, as well as the proposed modification of drag coefficient in Brahem, (2013).

The results with the VOF model did not finish, but maybe until the end of the simulation, when finished and stabilized, the water may come down to the initial position. The contours maybe show some entrainment of water in the gas, and the water is pushed against the walls (symmetric walls), and kept there was expected.

8 Bibliography

Alizadehdakhel, A., Rahimi, M., & Alsairafi, A. A. (2010). CFD and experimental studies on the effect of valve weight on performance of a valve tray column. *Cumputers and Chemical Engineering 34*, 1-8.

Brahem, R. (2013). *Étude de l'effet de l'échelle sur les plateaux à clapets de colonnes* . Toulouse: Institut de Mécanique des Fluides de Toulouse (IMFT).

Gamse, T. (2010). *Hydrodynamic Layout of Columns*. Graz: Graz University of Technology.

iea. (1973, April). *iea International Energy Agency*. Retrieved March 2014, from http://www.iea.org/statistics/

J.M.van Baten, R. (2000). Modelling sieve tray hydraulics using computational fluid dynamics. *Chemical Enginnering Journal 77*, 143-151.

Kolev, N. (2007). *Multiphase Flow Dynamics 2: Mechanical Interactions (Vol.2)*. Springer.

Lianghua, W., & Cui Juejian, Y. K. (2008). Numerical Simulation and Analysis of Gas Flow Field in Serrated Valve Column. *Chinese Journal of Chemical Engineering 16*, 541-546.

M., B., & I., T. (2009). Sweetening techologies- A look at the whole picture. *Word gas conference*. Argentina.

Rahimi, R. (2012). The effect of tray geometry on the sieve tray efficiency. *Chemical Engineering Science 76*, 90-98.

Stewart, M., & Arnold, K. (2011). *Gas Sweetening and Processing Field Manual*. USA: Elsevier Inc.

Stewart, M., & Arnold, K. E. (2011). *Gas Sweetening and Processing Field Manual* . USA: Elsevier Inc.

Yu, K. T. (1999). Computational fluid-dynamics and experimental verification of two-phase two-dimensional flow on a sieve column tray. *Chemical Engineering Research and Design 77(6)*, 554-560.

Zarei, A. R. (2012). A study on Sieve tray lower operating limit. *50th Distillation & Absorption Conference*, (pp. 479-484). Eindhoven, Netherland.

Zarei, A., Hossein, S. H., & Rahimi, R. (2012). CFD study of weeping rate in the rectangular sieve trays. *Journal of the Taiwan Institute of Chemical Engineers*.

Attachments

Correlation for gas retention

This Figure represents the different correlation for the gas retention.

Krishna et al (1999, 2000, 2003) Zarei et al (2012)	Bennett et l (1983) $\alpha_G^{Bennett} = 1 - e^{\left(-12.55\left(U_{G,s}\sqrt{\frac{\rho_G}{\rho_L-\rho_G}}\right)^{0.91}\right)}$
Gesit et al (2003)	Colwell (1979) $\alpha_G^{Colwell} = 1 - \frac{1}{1+\eta}$ $\eta = 12.6 Fr^{0.4}\left(\frac{A_h}{A_a}\right)^{-0.25}$ $Fr = \frac{\rho_G U_{Ga}^2}{\rho_L g h_{Lc}}$
Li et al (2009)	Li et al (2009) $\alpha_G^{Li} = 1 - e^{\left(-1.44\left(U_{G,s}\sqrt{\frac{\rho_G}{\rho_L-\rho_G}}\right)^{0.74}\right)}$
Jian et al (2012)	Jian et al (2012) $\alpha_G^{Jian} = 1 - e^{\left(-10.2\left(U_{G,s}\sqrt{\frac{\rho_G}{\rho_L-\rho_G}}\right)^{0.74}\right)}$

Figure 29- Empiric correlations of gas retention used in simulations Euler-Euler with the drag coefficient of Krishna et al. 1999 (Brahem, 2013)

Experimental Results of the two-phases

The experimental results have been done during the thesis of Rim Brahem. The height of clear liquid was estimated from the measurement of pressure drop at the emulsion. Different experimental works have been done for a range of gas kinetic factor Fa between 0 and 3.5. Different flowrate of liquid were tested. The clear liquid height increases by increasing the liquid flow.

For a fixed flowrate, two characteristic zones can be distinguished:

- First zone shows the increasing of h_{cl} with the augmentation of Fa. This zone is characterized by the high level of wepeening. The end of this zone is marked by a maximum of h_{cl}.
- The second zone is characterized by the decrease of h_{cl}.

Figure 30 represent the experimental values of h_{cl} dependent of Fa. (Brahem, 2013).

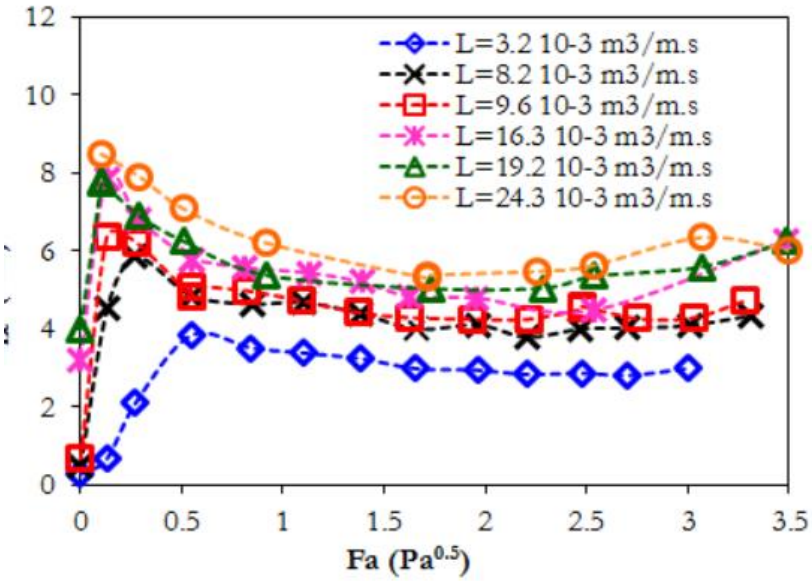

Figure 30-Experimental values of h_{cl} for different values of Fa.

The emulsion height was measure manually using pictures of the flow at different Fa. Figure 31 represent these measures for different flowrates.

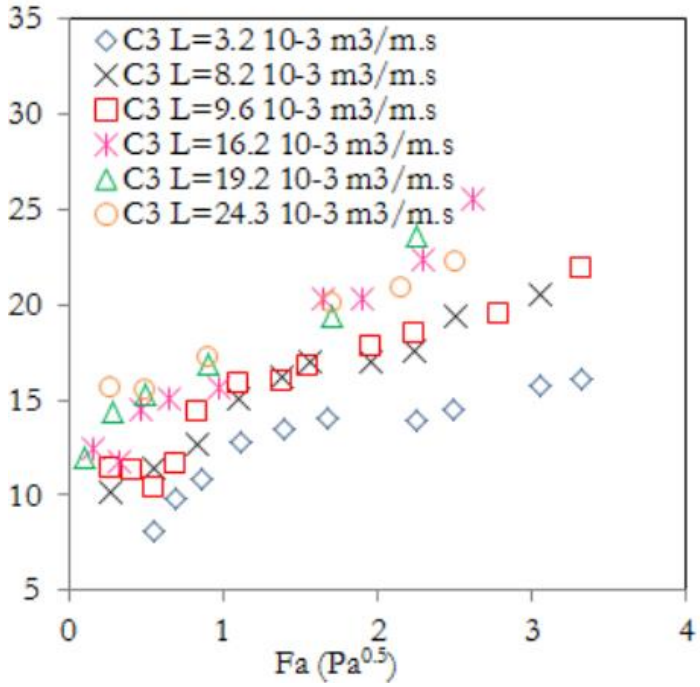

Figure 31- Measures of h_{Fe} for different flowrates and values of Fa between 0 and 4 $Pa^{0.5}$.

For the experimental results of liquid retention the results of emulsion height and clear liquid was used. So Figure 32 represents the liquid retention for different flowrate.

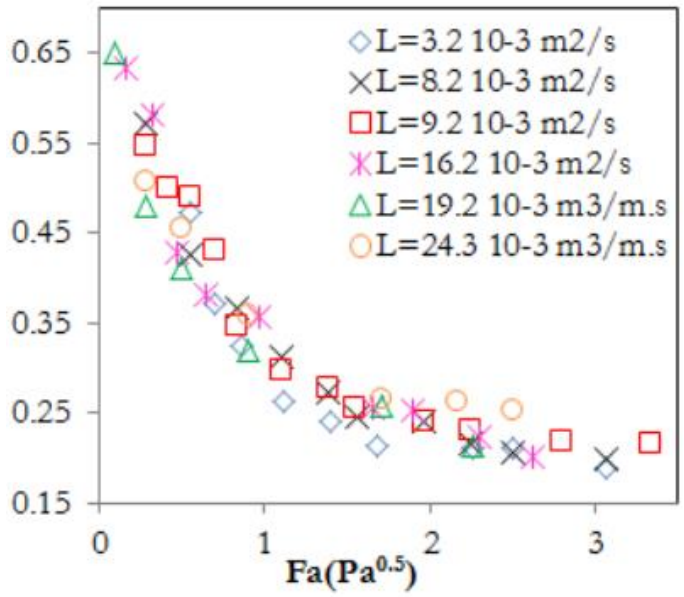

Figure 32- Experimental results of liquid retention in the column.

Degassing Condition

The degassing is applied in the outlet gas. This condition is available for two-phase liquid-gas flows using the Eulerian multiphase model. Is used to model a free surface through which dispersed gas bubbles are allowed escape but the continuous phase not. The continuous phase sees the outlet as a free-slip wall and does not live the domain.

VOF simulation geometry

The geometry is divided by 4 volumes to facilitate the patch:

- **First volume:** Is the tray, and the valve;
- **Second volume:** Represent the average height of the liquid in the tray during an experiment;
- **Third volume:** Correspond of weir height;
- **Fourth volume:** Represent the height between two trays and in the final of volume the exit of gas.

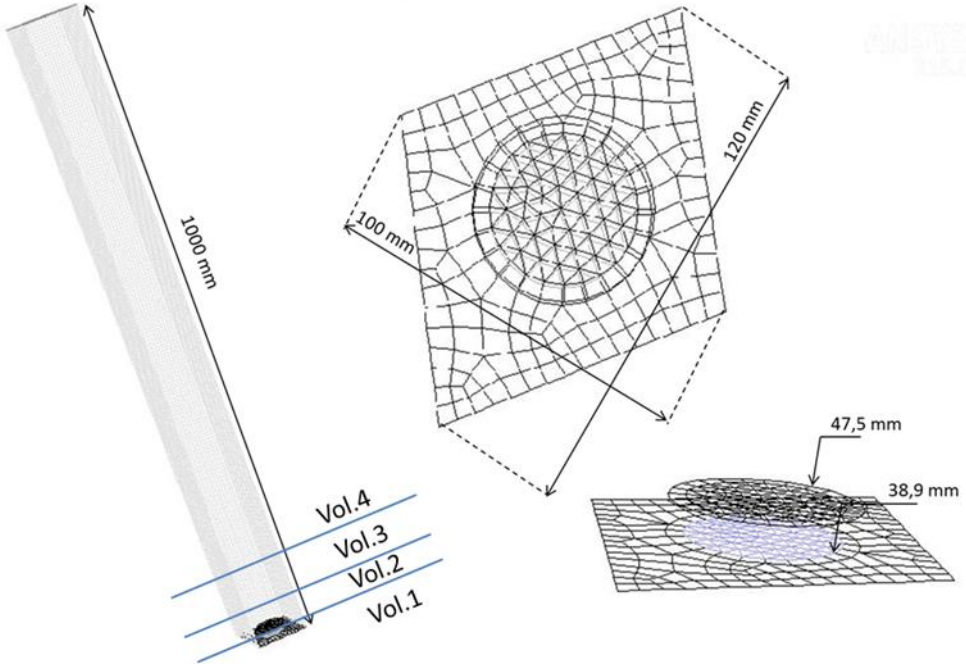

Figure 33-Scheme of geometry for the VOF model